NASA CONTRACTOR REPORT

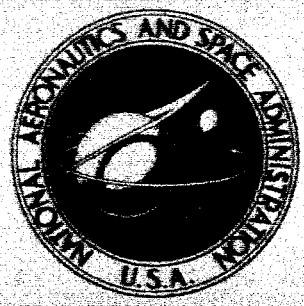

NASA CR-2438

NASA CR-2438

INVESTIGATION OF THE TURBULENT WIND FIELD BELOW 500 FEET ALTITUDE AT THE EASTERN TEST RANGE, FLORIDA

by Alfred K. Blackadar, Hans A. Panofsky, and Franz Fiedler

Prepared by
THE PENNSYLVANIA STATE UNIVERSITY
University Park, Pa. 16801
for George C. Marshall Space Flight Center

NATIONAL AERONAUTICS AND SPACE ADMINISTRATION • WASHINGTON, D. C. • JUNE 1974

TECHNICAL REPORT STANDARD TITLE PAGE

1. REPORT NO.	2. GOVERNMENT ACCESSION NO.	3. RECIPIENT'S CATALOG NO.
NASA CR-2438		

4. TITLE AND SUBTITLE	5. REPORT DATE
Investigation of the Turbulent Wind Field Below 500 Feet Altitude at the Eastern Test Range, Florida	June 1974
	6. PERFORMING ORGANIZATION CODE M131
7. AUTHOR(S) Alfred K. Blackadar, Hans A. Panofsky, & Franz Fiedler	8. PERFORMING ORGANIZATION REPORT #
9. PERFORMING ORGANIZATION NAME AND ADDRESS The Pennsylvania State University Department of Meteorology University Park, Pennsylvania 16801	10. WORK UNIT NO.
	11. CONTRACT OR GRANT NO. NAS8-21140
12. SPONSORING AGENCY NAME AND ADDRESS George C. Marshall Space Flight Center Marshall Space Flight Center, Alabama 35812	13. TYPE OF REPORT & PERIOD COVERED Contractor Final June 1971 - June 1973
	14. SPONSORING AGENCY CODE

15. SUPPLEMENTARY NOTES

This work was conducted under the technical monitorship of Dr. George Fichtl, Aerospace Environment Division, Marshall Space Flight Center, NASA, in support of the OAST Aeronautical Operating Systems Study Program.

16. ABSTRACT This report contains a detailed analysis of wind profiles and turbulence at the 150 m Cape Kennedy Meteorological Tower. It appears that the logarithmic law, in neutral air, and diabatic deviations from this law familiar from the surface layer, apply without systematic error up to 150 m. This analysis leads to a determination of roughness lengths, which are between 10 and 80 cm at Kennedy, depending on wind directions. Various methods are explored for the estimation of wind profiles, wind variances, high-frequency spectra and coherences between various levels, given roughness length, and either low-level wind and temperature data, or geostrophic wind and insolation. In the first case, the Monin-Obukhov length L_o is inferred from the winds and temperatures, and surface friction velocity is determined from the wind profiles. In the second case, theoretical relationships are first explored between geostrophic wind, surface Rossby number and surface stress. The relation between planetary Richardson number, insolation and geostrophic wind is explored empirically. The result is a nomogram for the determination of the planetary Richardson number. Techniques were devised which resulted in surface stesses reasonably well correlated with the surface stresses obtained from low-level data. Variances of the velocity components were well correlated with the surface stresses, but their vertical variations showed random behavior. No clear effect of stability on the variances was detected. Coherence between winds at different levels followed Davenport similarity with exponential decay as function of separation or frequency. The "slopes" for the lateral components were about twice those for the longitudinal components, in agreement with results elsewhere. Finally, based on all this information, practical methods are suggested for the estimation of wind profiles and wind statistics.

17. KEY WORDS	18. DISTRIBUTION STATEMENT
Atmospheric Turbulence Wind Shear Aircraft Response Aircraft Design and Operation	

19. SECURITY CLASSIF. (of this report)	20. SECURITY CLASSIF. (of this page)	21. NO. OF PAGES	22. PRICE
UNCLASSIFIED	UNCLASSIFIED	92	$4.00

MSFC - Form 3292 (Rev December 1972) For sale by National Technical Information Service, Springfield, Virginia 22151

TABLE OF CONTENTS

LIST OF FIGURES

LIST OF FIGURES (Continued)

LIST OF TABLES

FOREWORD

The research reported herein was supported by NASA Contract NAS8-21140. Dr. George H. Fichtl of the Aerospace Environment Division, Marshall Space Flight Center, was the scientific monitor, and support was provided by Mr. John Enders of the Aeronautical Operating Systems Office, Office of Advanced Research and Technology, NASA Headquarters.

The research reported in this document is concerned with the results of studies of wind and turbulence in the first 150 m of the atmospheric boundary layer. The motivation behind this research is the development of models of the statistical properties of atmospheric turbulence for the design and safe operation of aeronautical systems. Atmospheric turbulence models play a number of crucial roles in the design and operation of aeronautical systems. First, they provide for the development gust design criteria; second, they provide for the development of atmospheric turbulence simulation procedures whereby control systems can be evaluated and pilots can be trained. Finally, they provide a basis whereby the current requirements, criteria, and procedures for reporting winds and turbulence to pilots prior to take-off or the final approach can be evaluated, updated and improved, as well as for the development of possibly needed new procedures

It is believed that the models reported herein will contribute significantly to these areas of aeronautical interest, especially to the development of atmospheric turbulence simulation procedures.

I. INTRODUCTION

Certain statistics of airflow near the ground are of special interest to designers of aeronautical and aerospace vehicles and systems. These include the mean wind profile; variances of the velocity components; spectra of the velocity components and of dynamic pressure; and cospectra between velocity components at different levels. These quantities will be called "predictands". Two sets of "predictors" will be considered: either, conditions close to the ground measured locally; or large-scale data available from weather maps and astronomical tables.

The problem of estimating the predictands at Cape Kennedy from local variables has been discussed in previous reports, and will be summarized only briefly here. In this report, emphasis is placed on the problem of estimating the statistics required from large-scale variables.

Monin-Obukhov theory predicts that the statistics of atmospheric flow over homogeneous terrain in equilibrium in the "surface layer" are completely determined by three parameters: the roughness length, z_o; the friction velocity, u_*; and the Monin-Obukhov length, L, defined by:

$$L = - \frac{u_*^3 \, c_p \, \rho \, T}{kgH} \qquad (1)$$

Hence, c_p is the specific heat at constant pressure, T temperature, ρ density, g gravity, k von Karman's constant, and H the vertical heat flux (including the effect of moisture on buoyancy).

The "surface layer" is defined as that region in which the vertical variation of u_*, H and therefore L can be neglected. This is approixmately true only in the lowest 30 m or so; the possibility remains, however, that the relationships valid in the surface layer may apply up to the top of the Kennedy tower (150 m), if surface values of friction velocity, heat flux and L could be inserted into these relations. The relations, and tests of their validity up to 150 m are discussed in Chapter IV.

The roughness length is needed in the estimation of the predictands both from local and from external variables. Therefore a separate chapter, Chapter II, is devoted to its determination at Cape Kennedy.

The determination of u_* and L from local variables has been discussed in earlier reports and will be summarized briefly in Chapter III. The estimation of the same quantitites from large-scale variables formed a major part of this project, and is discussed both on the basis of theory and measurements in Chapter V.

Combination of the results of Chapter II, III, and V leads to techniques for estimation of the predictands from large-scale variables only. These methods, and a test of their accuracy, are given in Chapter VI. Chapter VII gives instructions for the estimation of the various statistics from usually observed data. Finally, an appendix discusses statistical and mathematical properties of time series of atmospheric turbulence at Cape Kennedy and elsewhere.

The tower and instrumentation at Cape Kennedy will not be described in detail here, since this has been done by other authors, e.g., by Fichtl and

McVehil (1970). Suffice it to say here that mean and fluctuating wind, as well as mean temperatures were available at six levels: 18 m, 30 m, 60 m, 90 m, 120 m and 150 m.

Some of the material in this report has been discussed in two previous reports, NASA CR-1410 and NASA CR-1889; these will be referred to as Reports 1 and 2, respectively.

II. DETERMINATION OF ROUGHNESS LENGTH AT CAPE KENNEDY

Roughness length is usually determined from wind profiles, preferably under neutral conditions, although alternative methods have been suggested in earlier reports. Determination of roughness lengths from wind profiles presupposes a thorough understanding of profile theory, above the surface layer. At the time of writing of this report, numerous profiles have been processed so that their properties could be evaluated sufficiently well to suggest reliable estimates of roughness lengths. To simplify matters, only neutral conditions are considered first. This is accomplished by considering only average profiles of individual runs, for which the Richardson number between 18 and 30 m lies between -.05 and +.05.

Up to 150 m, it is presumably legitimate to obtain equations for the wind profile under the assumption that the wind direction is invariant with height. Then, we may derive expressions for the profile over homogeneous terrain by integration of the differential equation for wind u as a function of height z:

$$\frac{du}{dz} = u_*/\lambda \qquad (2)$$

This equation may be considered as the definition of the "mixing length", λ. The quantity u_* is the local friction velocity. Of course in the surface layer, the friction velocity is constant and $\lambda = kz$, so that the wind follows the familiar logarithmic relation.

The behavior of the friction velocity above the friction layer can be derived rigorously from the equation of motion in the direction of the wind:

$$2u_* \frac{du_*}{dz} = fv_g \tag{3}$$

Here, v_g is the component of geostrophic wind at right angles to the surface wind u, and f is the Coriolis parameter.

From the theory of the geostrophic drag coefficient (see, for example, Blackadar and Tennekes, 1968), we have

$$v_g/u_{*o} = -\frac{B}{k} \tag{4}$$

Here B varies with stability. Under neutral conditions the best estimate for B is about 5 (for further discussion, see Chapter V). Integration then shows that, very nearly

$$u_* = u_{*o} - 6fz \tag{5}$$

where u_{*o} is the friction velocity at the surface.

Since the mixing length, λ, is kz near the ground, and applying the scaling appropriate for the neutral planetary boundary layer, we may put:

$$\lambda = kz\ F\ (\frac{fz}{u_{*o}}) \tag{6}$$

Here F is presumably a universal function. For example, Blackadar (1962) has suggested:

$$F = (1 + 63\ \frac{fz}{u_{*o}})^{-1} \tag{7}$$

If we now substitute equations (5) and (6) into (2), and integrate, we may write formally:

$$u = \frac{u_{*o}}{k} \left[\ln \frac{z}{z_o} + G \left(\frac{fz}{u_{*o}} \right) \right] \tag{8}$$

where $G(\frac{fz}{u_{*o}})$ is another universal function, related to F. In particular, with Blackadar's hypothesis for F, the expression for the wind profile can be written

$$u = \frac{u_*}{k} \ln \frac{z}{z_o} + 144\ fz \tag{9}$$

Figure 1 shows the logarithmic wind profile, and, for comparision, (9) with roughness length 20 cm and friction velocity 52 cm/sec. Clearly, the Blackadar profile in semilogarithmic representation curves significantly in the lowest 100 m.

Geometrically, the roughness length is given by the intercept of the profile with the ordinate. In practice, however, the roughness length is often determined by constructing a tangent to the observed portion of the profile and determining z_o from its intercept with the ordinate, a procedure based on the assumption of a logarithmic wind profile. Clearly, if the actual profile is as strongly curved as Blackadar's profile, the roughness length would then be strongly overestimated. It is therefore of great importance to analyze profiles observed under hydrostatically neutral conditions in order to study their curvature.

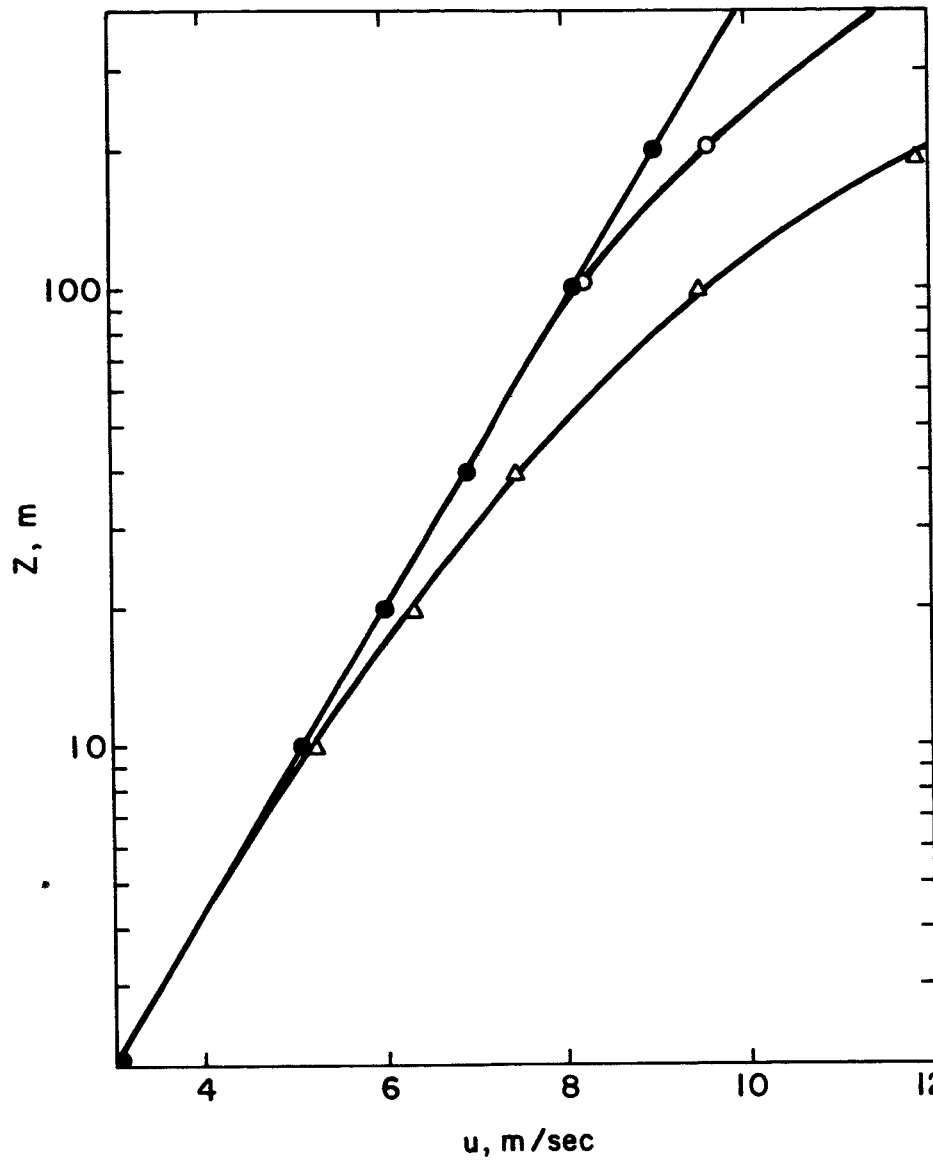

Figure 1. Theoretical wind profiles for 20 cm roughness length and u_{*o} = .52 m. • = logarithmic law, o = log-linear law, Δ = hyperbolic sine law.

Ten-minute average wind profiles are now available on tape, one for every hour of 1968. From these, mean "neutral" profiles regardless of wind speed were computed, for twelve wind direction sectors. Here, "neutral" is defined by $-.05 < Ri < +.05$. The resulting profiles are shown in Figure 2.

It is clear that the twelve profiles show considerable irregularities, but no systematic bending to the right with increasing height. This result is in agreement with conclusions reached by Thuillier and Lappe (1964) who analyzed profiles near Dallas, Texas. Many of the irregularities may be due to instrument effects; in a few cases, as will be seen, the change of terrain upstream of the tower may be responsible for kinks in the profiles.

In any case, (9) does not provide the best fit to the observations. A somewhat better fit is provided by the hypothesis

$$\lambda = 0.0063 \frac{u_{*o}}{f} \tanh \frac{kzf}{0.0063\ u_{*o}} \qquad (10)$$

which leads to geostrophic drag coefficient statistics in as good agreement with observations as (7). In that case, the wind profile can be written, omitting a term in $(fz)^2$

$$u = \frac{u_{*o}}{k} \ln \frac{\sinh 63\ fz/u_{*o}}{\sinh 63\ fz_o/u_{*o}} - 15\ fz \qquad (11)$$

This wind profile is also shown in Figure 1. It is quite close to the logarithmic profile and, when fitted to observed profiles, should produce better roughness lengths than (9); but the results should not necessarily be

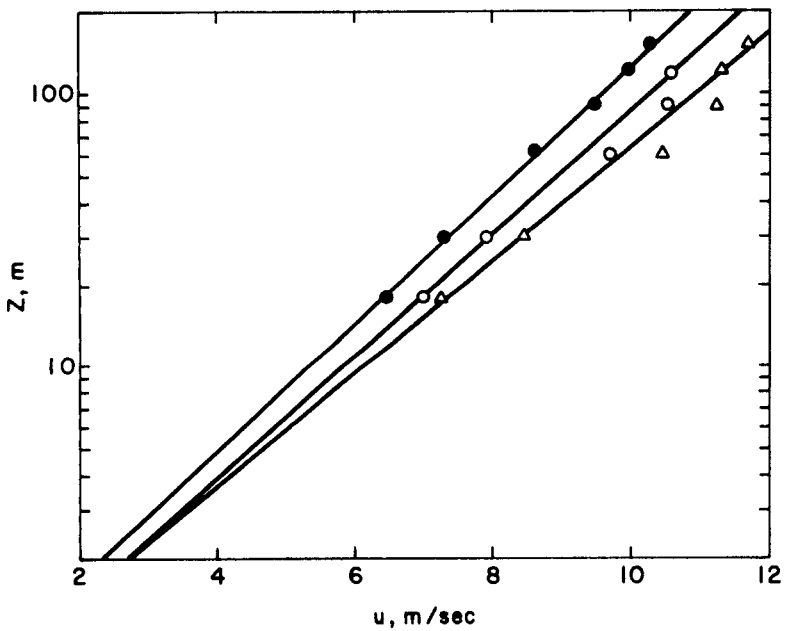

Figure 2a. Neutral wind profiles at Cape Kennedy for wind directions • 225°, o 0285°, and Δ 255°.

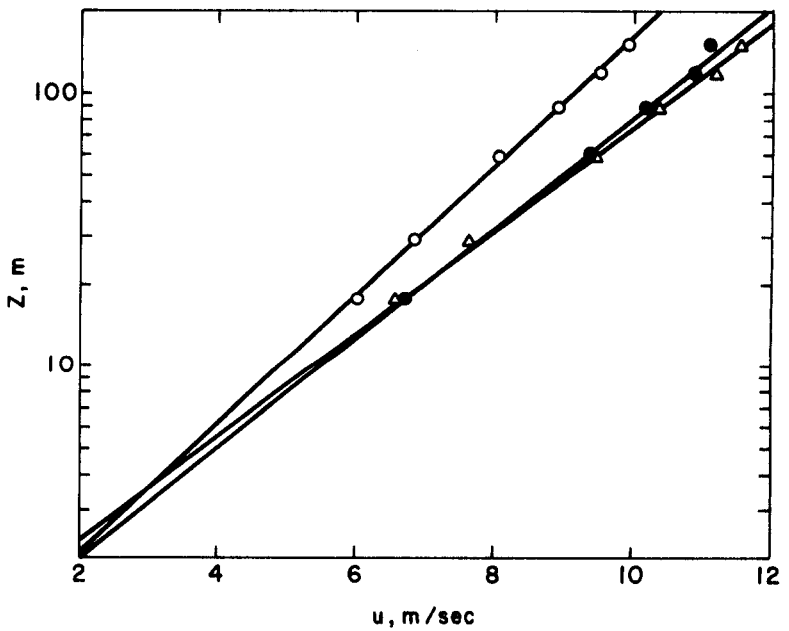

Figure 2b. Neutral wind profiles at Cape Kennedy for wind directions 0 195°, Δ 165°, and • 135°.

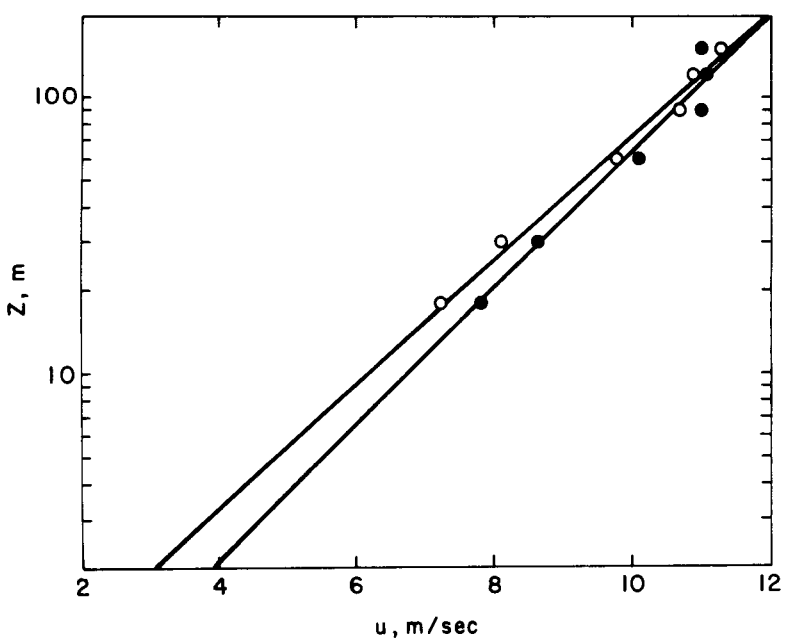

Figure 2c. Neutral wind profiles at Cape Kennedy for wind directions o 315°, • 345°.

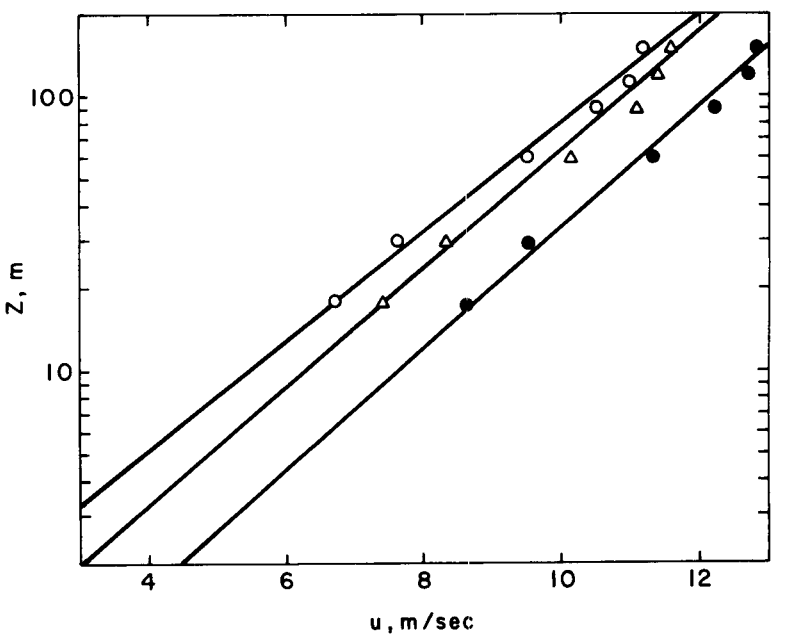

Figure 2d. Neutral wind profiles at Cape Kennedy for wind directions o 105°, Δ 75°, • 45°.

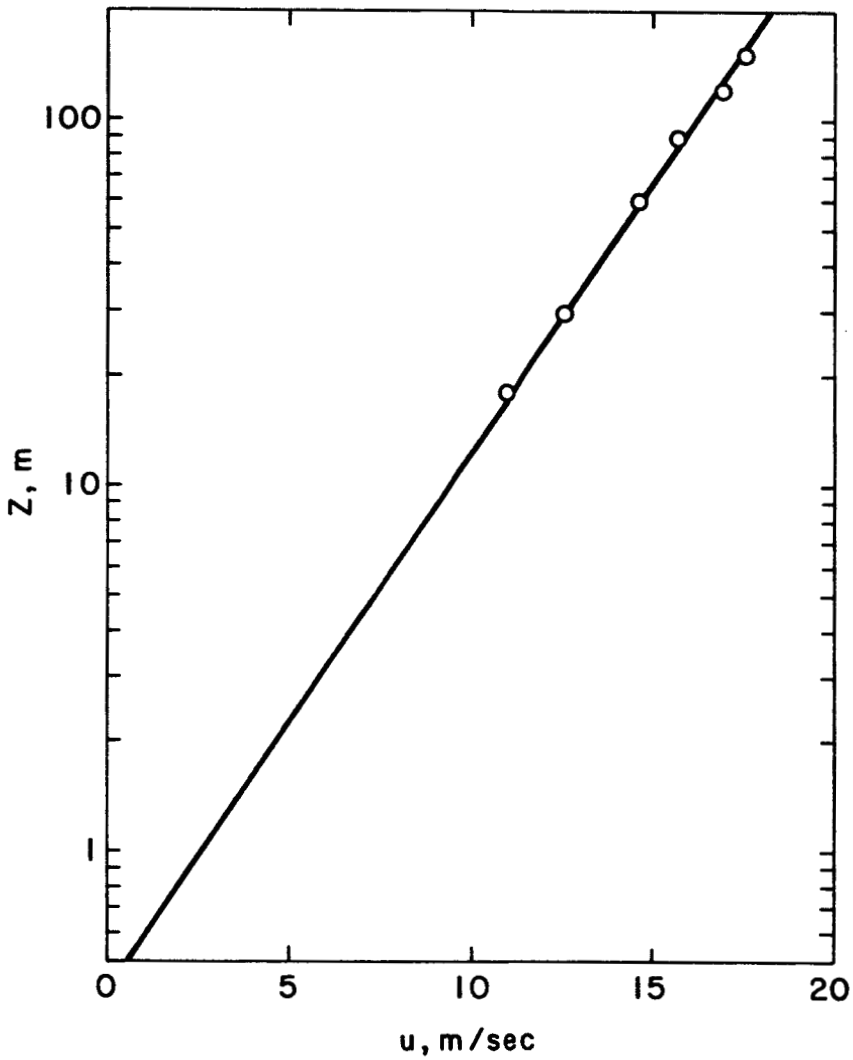

Figure 2e. Neutral wind profile at Cape Kennedy for wind directions 15°.

superior to roughness lengths determined under the assumption of a logarithmic profile. Because computations based on the assumption of logarithmic profiles are by far the simplest, logarithmic relations were assumed.

Actually, two sets of roughness lengths were obtained from the near-neutral wind profiles: first, lines were fitted to the profiles shown in Figure 2; and second, average profiles were constructed from fewer individual profiles, the Richardson number of which was restricted to lie between -.01 and .01. Thus, usually ten or fewer individual ten-minute profiles were averaged in each wind direction sector. The random errors in these averages are larger than in the first sample, but systematic errors should be smaller. Generally, the agreement between the two sets of roughness lengths was quite good, and they were averaged.

Two other groups of roughness lengths were used, both requiring theoretical expressions for the correction to the logarithmic wind profiles due to unstable stratification. The characteristics of these expressions are quite well known for the surface layer, generally taken as the layer below 30 m or so. Panofsky and Petersen (1972) have recently tested the hypotheses that the expressions valid below 30 m can be applied up to 100 m, on the basis of observations at Risø, Denmark. The results were favorable to the hypothesis. An independent test will now be described which was made on Kennedy profiles. This was based on hour-average mean profiles, in various categories of L_o, the Monin-Obukhov length. The average profiles themselves, along with the mean value of L_o for each, are shown as Figure 3. Again, the "neutral" profile is logarithmic, with an intercept suggesting a mean roughness length of 0.4 m. The other profiles have the expected curvatures.

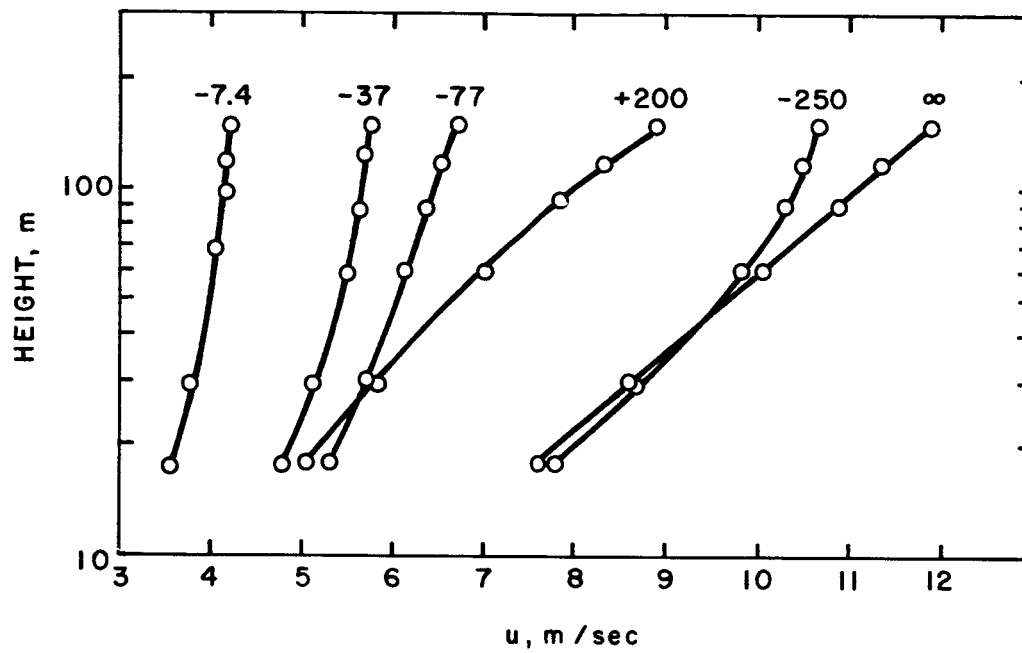

Figure 3. Average wind speed profiles of one-hour runs, from left to right, at 150 m: L = - 7.4 m, L = - 37 m, L = - 77 m, L = + 200 m, L = - 250 m, L ~ ∞.

The test was made on the basis of the nondimensional vertical wind shear,

$$\phi = \frac{kz}{u_*} \frac{du}{dz} \tag{12}$$

In the surface layer, and, according to the hypothesis, up to 100 m, in unstable air

$$\phi = (1 - 16\ z/L_o)^{-1/4} \tag{13}$$

In practice, normalized wind shears were computed by dividing wind differences between successive levels Δu_u by the corresponding wind differences Δu_n under neutral conditions. Since $\phi = 1$ in neutral air,

$$\phi_u/\phi_n = \phi_u = \frac{u_{*no}}{u_{*_o}} \frac{\Delta u_u}{\Delta u_n} \tag{14}$$

Subscripts u and n denote unstable and neutral, respectively. The ratio u_{*no}/u_{*uo} was evaluated from equation (15) (see below) applied at 18 m:

$$\frac{u_{*no}}{u_{*uo}} = \frac{u_{n_{18}}}{u_{u_{18}}} \left(1 - \frac{\psi(\frac{18}{L_o})}{\ln \frac{18}{z_o}}\right)$$

This procedure for evaluating ϕ has the advantage that it eliminates systematic errors in wind measurements caused by systematic changes of roughness with distance from the tower. The determination of the Monin-Obukhov length L_o is described in the next chapter. The same technique had been used successfully with Risø wind profiles.

Figure 4 compares the theoretical dependence on ϕ on z/L_o with the observations. Some observations from the Risø tower (Denmark) are included. The agreement is surprisingly good, and further confirms the hypothesis that (13) can be used up to 100 m, or even to slightly greater heights. Thus, the method for determining surface stress and roughness suggested by Panofsky (1963) can be applied to the tower data.*

First, the diabatic wind profile is written as:

$$u = \frac{u_{*o}}{k} [\ln (ze^{-\psi}) - \ln z_o] \qquad (15)$$

Paulson (1970) determined ψ for unstable air from (13):

$$\psi \left(\frac{z}{L_o}\right) = \ln \frac{2z}{L_o} \left(\frac{1+x}{1-x}\right) - 2 \tan^{-1} \left(\frac{z}{L_o}\right) + \frac{\pi}{2} \qquad (16)$$

Here $x = (1 - 16\ z/L_o)^{1/4}$. Equation (15) is a linear equation between u and $\ln(ze^{-\psi})$, with $\ln z_o$ as intercept. In stable air, we take $\psi = -5\ z/L_o$. Table 1 lists ϕ, ψ and $e^{-\psi}$ computed from these equations.

---

*More recent data from Idaho Falls as well as the points plotted suggest that a better fit is given by the KEYPS equation

$$\phi^4 - 18 \frac{z}{L_o} \phi^3 = 1$$

which also has the property that, as $-z/L_o \to \infty$, K_m is independent of z_o and u_{*o}, as required by the original theory of free convection. Another excellent fit, undistinguishable here from the KEYPS equation, is provided by:

$$\phi = \left(1 - 18 \frac{z}{L_o}\right)^{-1/3}$$

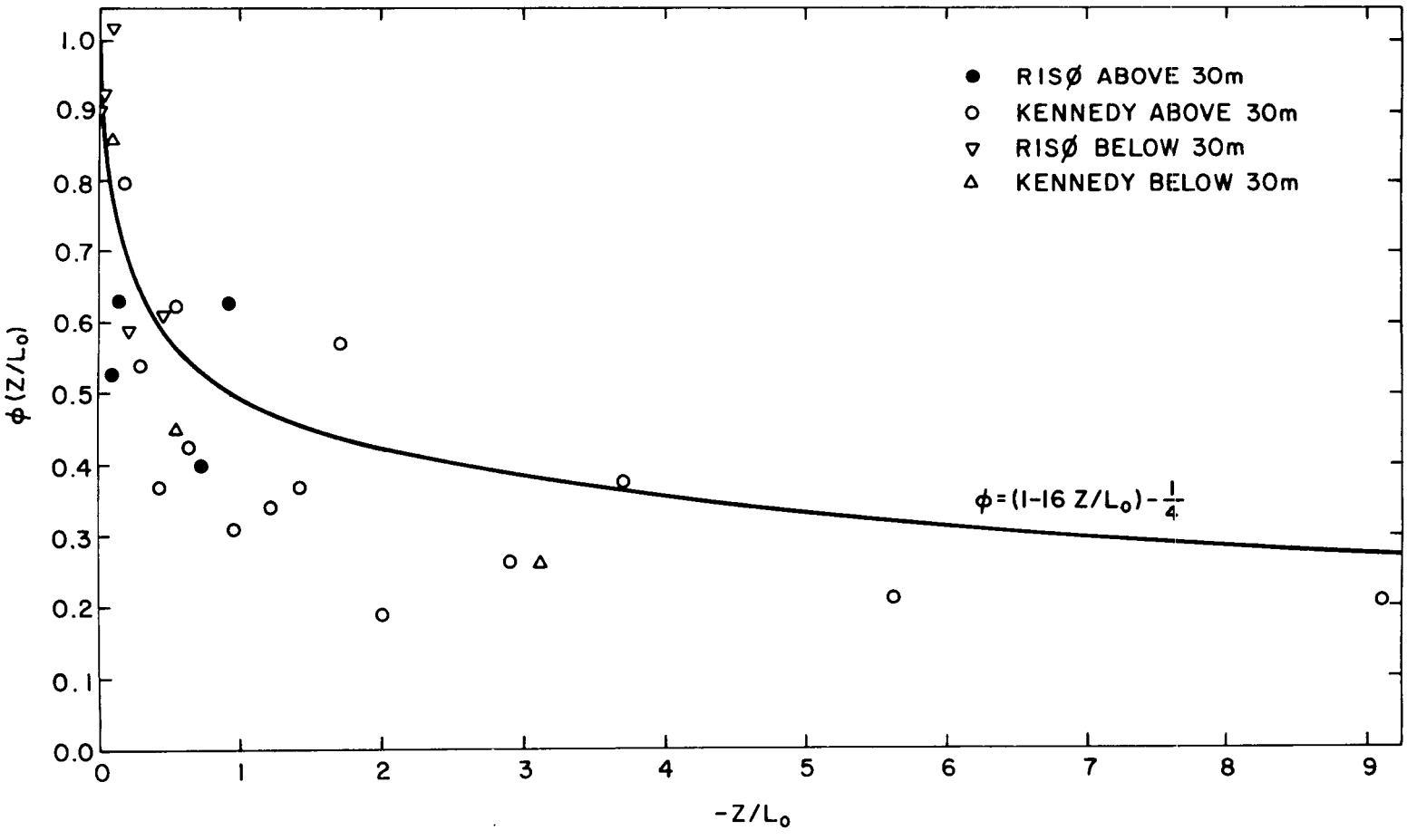

Figure 4. Observations of $\phi = \frac{kz}{u_{*_o}} \frac{\partial u}{\partial z}$ vs $- z/L_o$ compared with Businger hypothetical curve.

Table 1. Wind profile parameters ϕ, ψ, and $e^{-\psi}$ as functions of z/L_o

z/L_o	0.1	0.05	0	-.1	-.2	-.3	-.4	-.5	-.6	-.7	-.8	-.9	-1	-2	-3
ψ	-0.5	-0.25	0	.28	.45	.59	.70	.79	.87	.94	1.01	1.06	1.12	1.49	1.74
$e^{-\psi}$	1.65	1.28	1.0	.75	.64	.55	.50	.45	.42	.39	.37	.35	.33	.22	.18
ϕ	1.50	1.25	1.0	.79	.70	.65	.61	.58	.56	.54	.52	.50	.49	.42	.38

Average wind profiles were constructed from the 10-minute average winds in 1968 for each sector, and (15) was fitted to each by least squares. This yielded the second set of roughness lengths. The third set was that given by Fichtl and McVehil (1970) which was based on one-hour average winds, but only at 18 m and 30 m. The first two sets then effectively represent average roughness lengths applying to the whole tower, whereas the third set represents the lowest section of the tower.

All three sets of roughness lengths are shown in polar form in Figure 5. Also, a line is drawn into the figure, which is taken to be the "best" distribution of roughness lengths at Cape Kennedy. The three sets agree quite well with each other, with that by Fichtl and McVehil yielding slightly lower values than the others. This is because the average logarithmic wind shear between 18 m and 30 m is very slightly smaller than higher up, suggesting slightly smaller roughness lengths in the immediate neighborhood of the tower than further away.

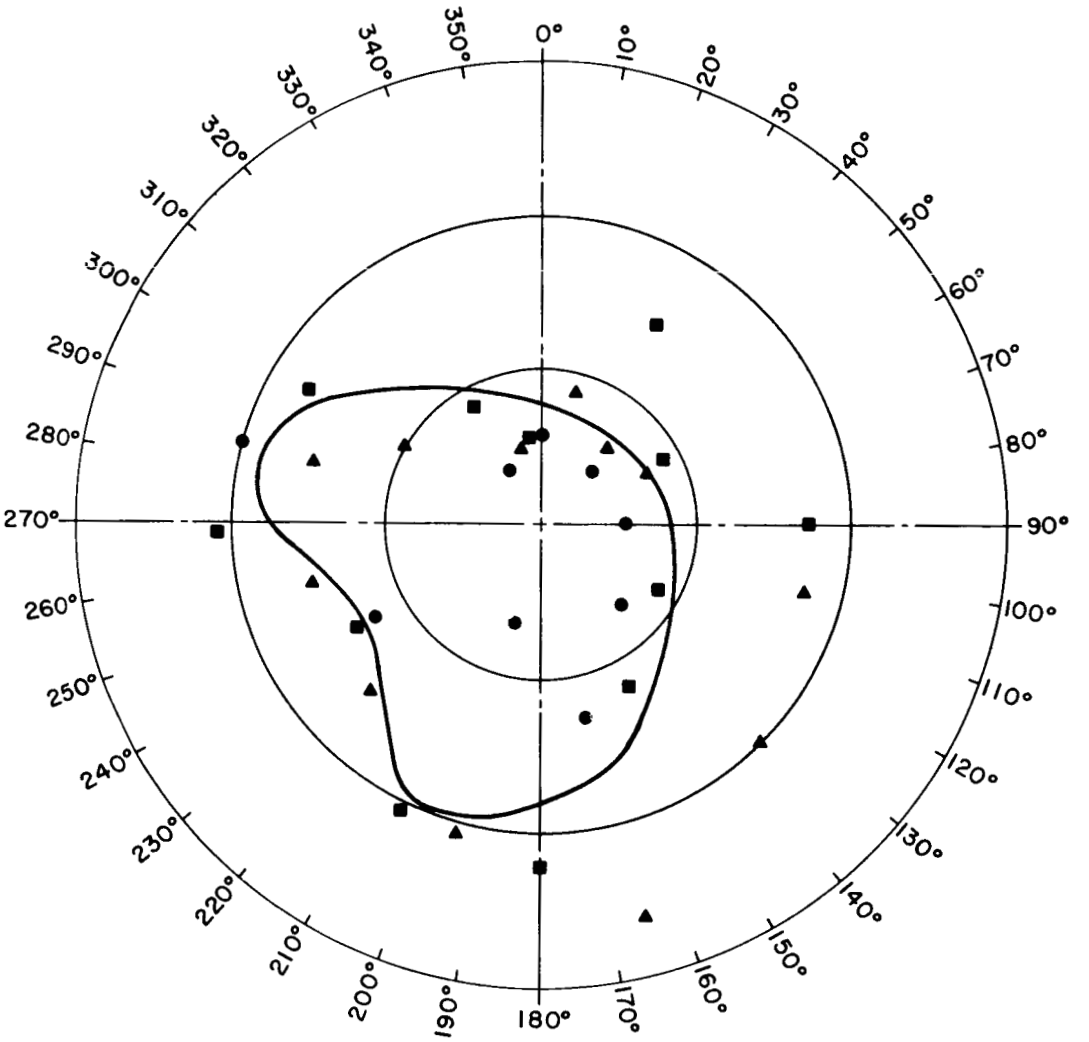

Figure 5. Polar diagram of roughness lengths
Δ neutral only, ten minute average wind
■ neutral and unstable, 1 hour averages
• Fichtl and McVehil

A qualitative test of the roughness lengths involves comparing their angular distribution with the corresponding distribution of terrain features. Fichtl and McVehil (1970) distinguish basically two sectors: essentially smooth terrain (vegetation 0.5 to 1.5 m high) from 300° through 360° to 160°; and a sector with trees about 200 m and more from the tower, from 160° through south to 300°. The "smooth" area is interrupted by a narrow band of trees 450 m away to the east and southeast. It is seen that the angular distribution of roughness lengths shown in Figure 5 agrees fairly well with the terrain.

West of the tower, and about 200 m from it, there is a strip of forest extending to a distance about 400 m from it. The wind profiles for wind directions 255° and 285° in Figure 2 both show a large wind shear between 30 m and 60 m, corresponding to roughness lengths of about 1.5 m. This roughness length is about what would be expected for woods, and the heights of the large-shear layer are consistent with theory (Elliott, 1958) and observations elsewhere. Similar irregularities in the wind profiles are found with easterly winds, which may be due to a small hill in that direction. Nevertheless, this explanation of profile irregularities must be considered as extremely tentative.

In summary, the angular distribution of roughness lengths, as shown in Figure 5, is in reasonably good agreement with terrain characteristics. However, it will be seen later that these roughness lengths are generally larger than what would have been expected from the fluctuation statistics.

The roughness lengths discussed in this chapter are essentially "local" roughness lengths. Having been obtained from wind profiles up to 150 m at a tower, they represent approximately a circle of radius 1 km, with the tower

at its center. For applications to the dynamic behavior of rockets on the pad and shortly thereafter, such local roughness lengths are needed, in contrast to requirements for the estimation of the effect of terrain on airplanes, or on large-scale momentum transfer.

If the relations valid at Cape Kennedy are to be applied elsehwere, analogous "local" roughness lengths must be estimated. Only approximate guidelines can be stated for such quantities: 10^{-2} cm for unobstructed water surfaces; 1-10 cm for low grass and low vegetation; 10-80 cm for fields broken by trees and hours; 80-400 cm for mainly forested regions and cities. These estimates are still controversial and require considerable refinement.

III. DETERMINATION OF L_o AND u_{*o} FROM LOW-LEVEL VARIABLES

According to Monin-Obukhov theory, the meteorological predictands needed for the design and operation of aeronautical and aerospace systems can be estimated as function of roughness length, friction velocity and Monin-Obukhov length in the surface layer over homogeneous terrain. Before tests can be made to what extent these relations are valid up to the top of the Kennedy tower, at 150 m, estimates of L_o, z_o and u_{*o} first have to be made. In the last chapter, the characteristics of roughness length were described. Here, the question of the estimation of L_o and u_{*o} will be taken up.

According to theory, z/L_o in the surface layer is a universal function of the Richardson number, Ri, defined by

$$Ri = \frac{g}{T} (\gamma_d - \gamma)/(\frac{du}{dz})^2 \qquad (17)$$

Here, γ is the lapse rate of temperature, and γ_d the adiabatic lapse rate. Observations at well instrumented, homogeneous sites (see, e.g. Paulson 1970) confirm the hypothesis, proposed originally independently by Pandolfo, Dyer and Businger, that Ri and z/L_o are essentially equal to each other in unstable air, so that we may put:

$$L_o = z/Ri \qquad (18)$$

In stable air, the Monin-Obukhov hypothesis is more controversial, but a good relation (for $Ri << .20$) seems to be

$$L_o = z \left[\frac{1}{5Ri} - 1\right] \tag{19}$$

(see Businger, et al., 1971).

The Richardson number appearing in (18) and (19) has usually been determined directly from its definition (17) from observations of wind and temperature at 18 m and 30 m; z in the equations is taken as the geometric mean of these two heights or 23 m. Although this technique has actually been used in this project for determining L_o, it probably is not the best technique because it involves the squares of measured wind shears which have large observational uncertainties.

A better method for obtaining Ri involves measurement of the bulk Richardson number. The bulk Richardson number is defined by:

$$B = g \frac{\gamma_d - \gamma}{T} \left(\frac{z^2}{u^2}\right) \tag{20}$$

which can be determined with much greater percentage accuracy than Ri, because u has a much smaller percentage error than du/dz.

Ri is connected with B through

$$Ri = B \left[u / \frac{du}{d(\ln z)}\right]^2 \tag{21}$$

Given ϕ and ψ from (12) and (15) respectively, we have:

$$Ri = B \left[\frac{\ln z/z_o - \psi}{\phi}\right]^2 \tag{22}$$

For the surface layer, both ψ and ϕ are now quite well known (see Chapter II), and therefore it is possible to construct a nomogram for Ri as a function of B and z/z_o. This nomogram is shown in Figure 6.

Figure 7 compares values of Ri from (17) with those computed from Figure 6 for O'Neill, where winds are extremely accurate. The agreement is excellent.

Figure 8 shows the same kind of comparison for Cape Kennedy from winds and temperatures at 18 m and 30 m. The height z was taken as 23 m, the geometric mean. The value of z_o was obtained by plotting $\ln z - \psi$ as function of u from 18 m to 30 m and locating the intercept of the straight line through the two points.

Figure 8 shows that a line of slope 45° fits the data as well as any line, suggesting no systematic error. But the scatter is enormous, suggesting large random errors in the "measured" Ri. That Ri-values are uncertain is confirmed by the wind profiles described in Chapter II.

It is therefore concluded that L_o can be found from bulk Richardson number and Figure 6 more accurately than by direct measurement. If lapse rate is not available, we may use the Pasquill stability classes (Table 2) taken from Slade (1968). Only rough estimates of wind and radiation conditions are required to determine these classes. The classes can be combined with roughness length to arrive at an estimate of L_o using Figure 9, which has been taken from Golder (1972).

Finally, if radiation and wind at a low level are given, L_o can be found from Figure 10, which, however, has been derived from Kennedy data only and is not necessarily valid elsewhere.

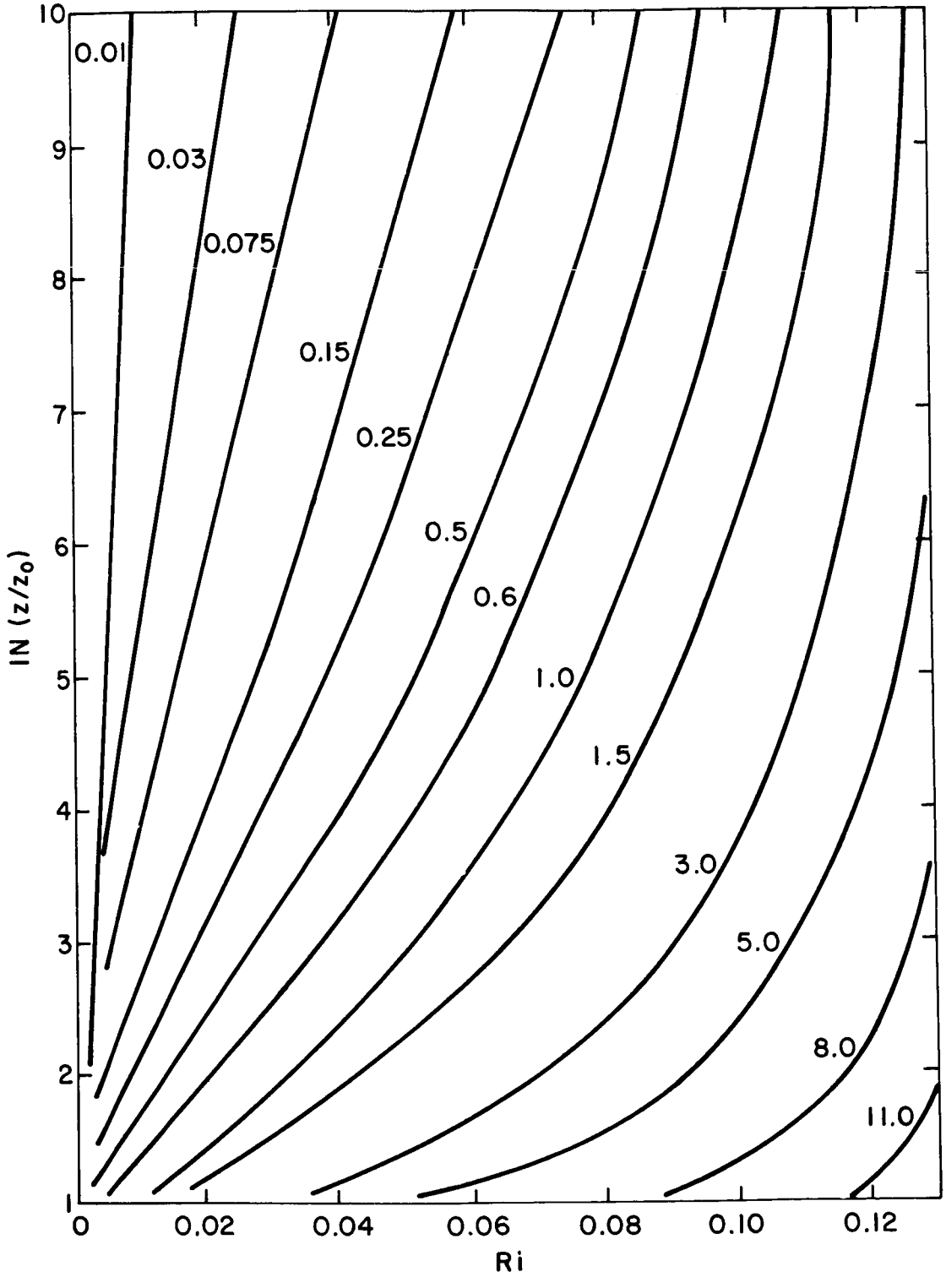

Figure 6a. Nomogram for Richardson number as function of bulk Richardson number B and z/z_o (stable).

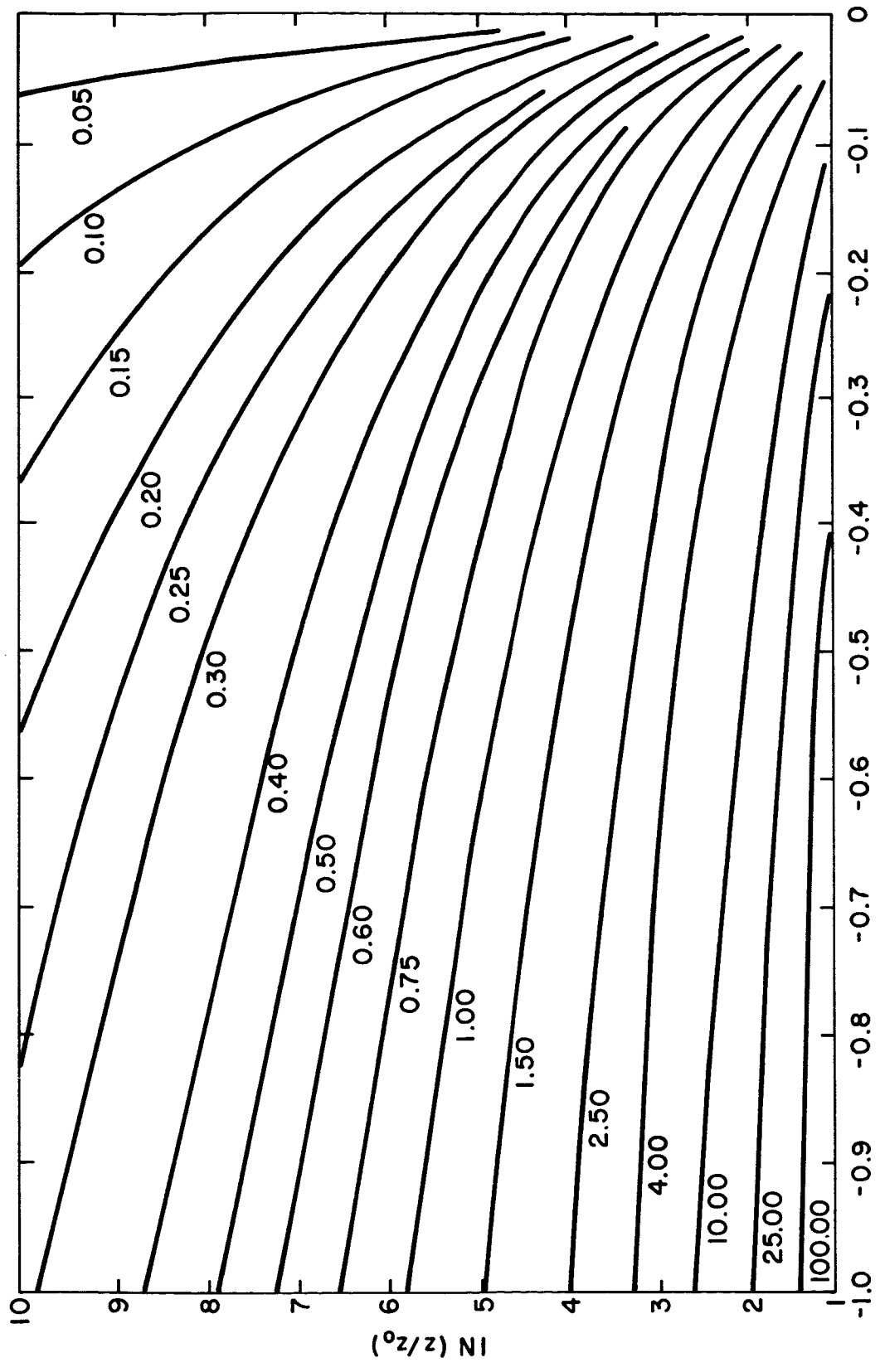

Figure 6b. Nomogram for Richardson number as function of bulk Richardson number B and z/z_o (unstable).

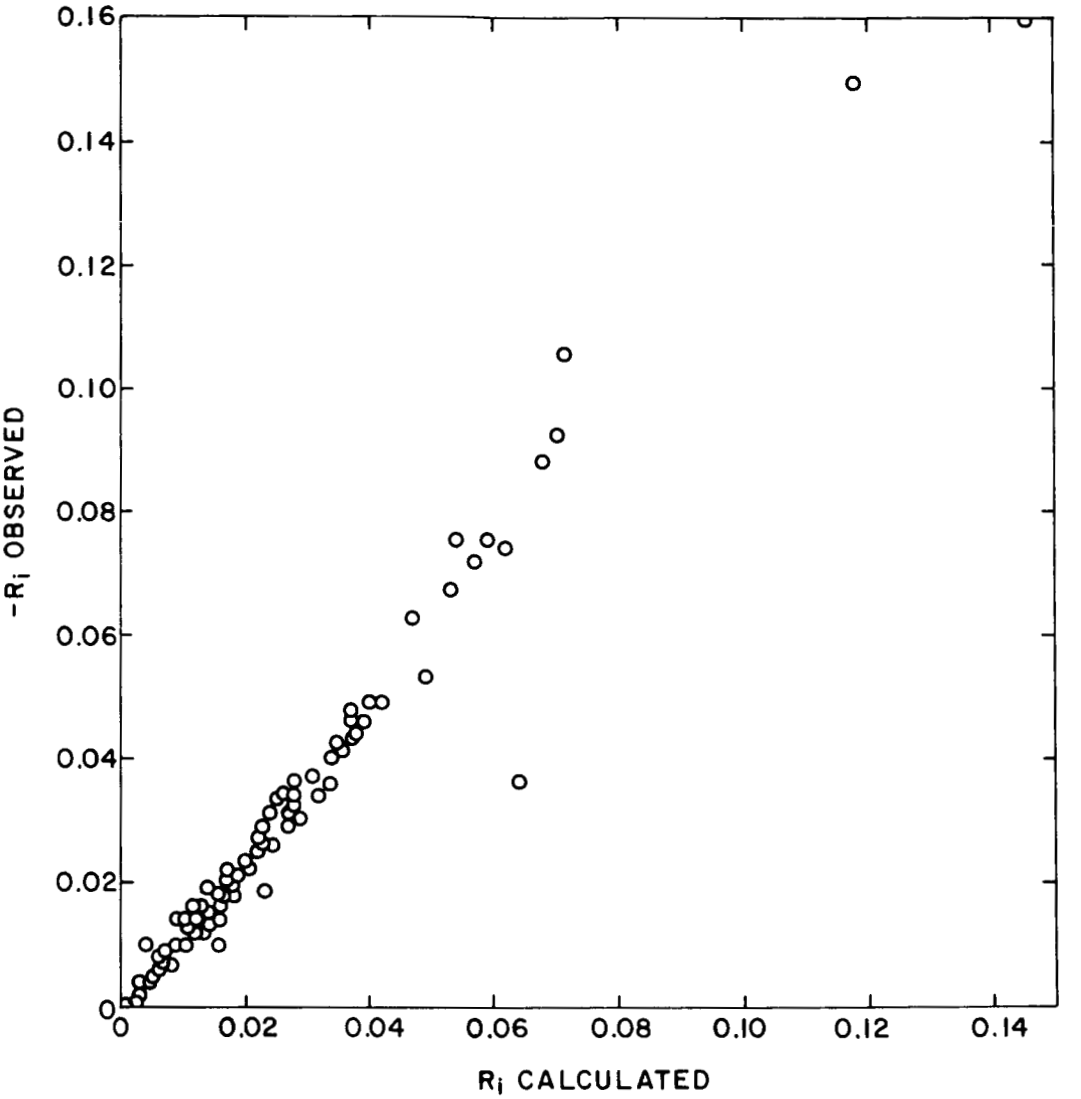

Figure 7. Observed and calculated Ri, O'Neill.

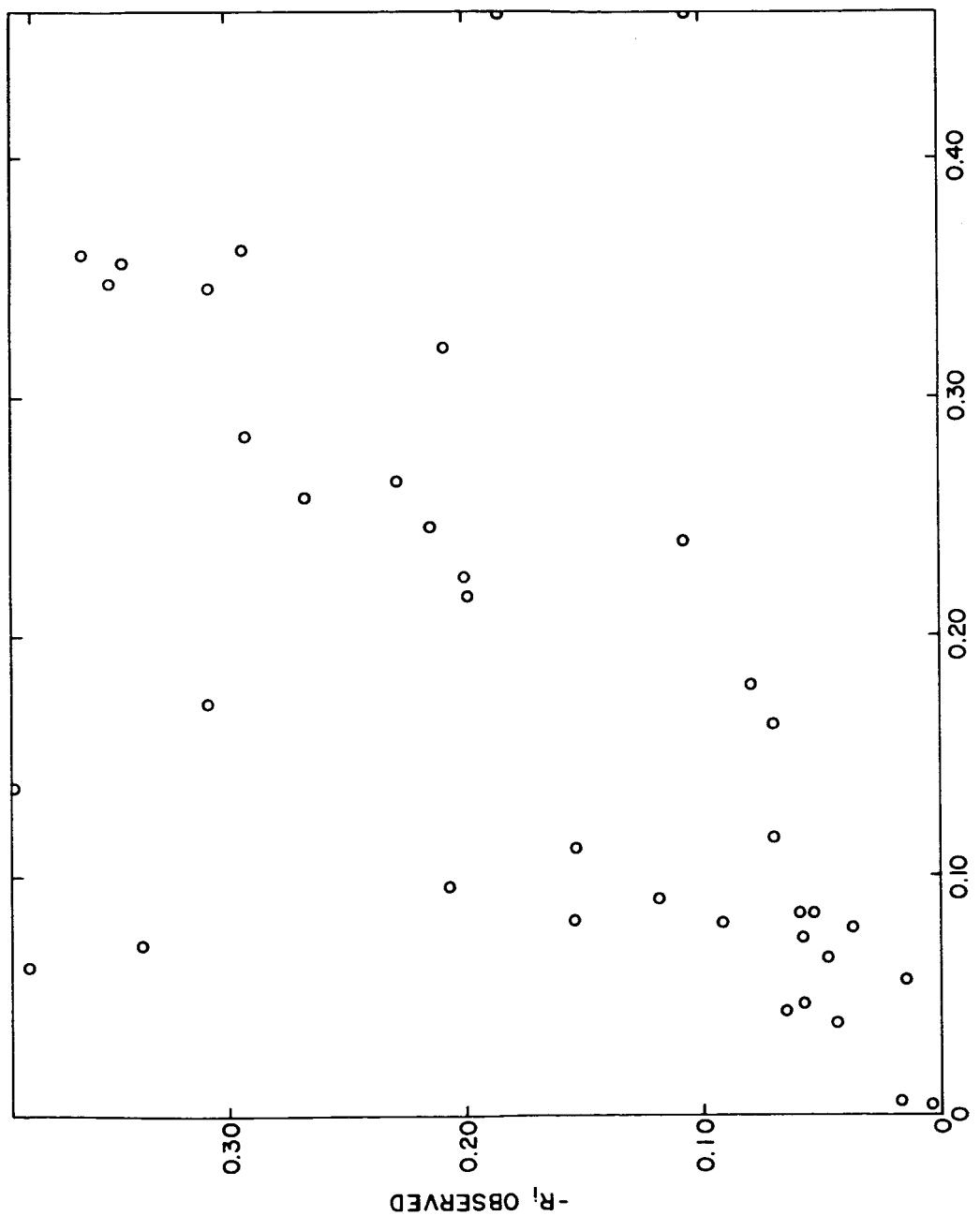

Figure 8. Observed and calculated Ri, Cape Kennedy.

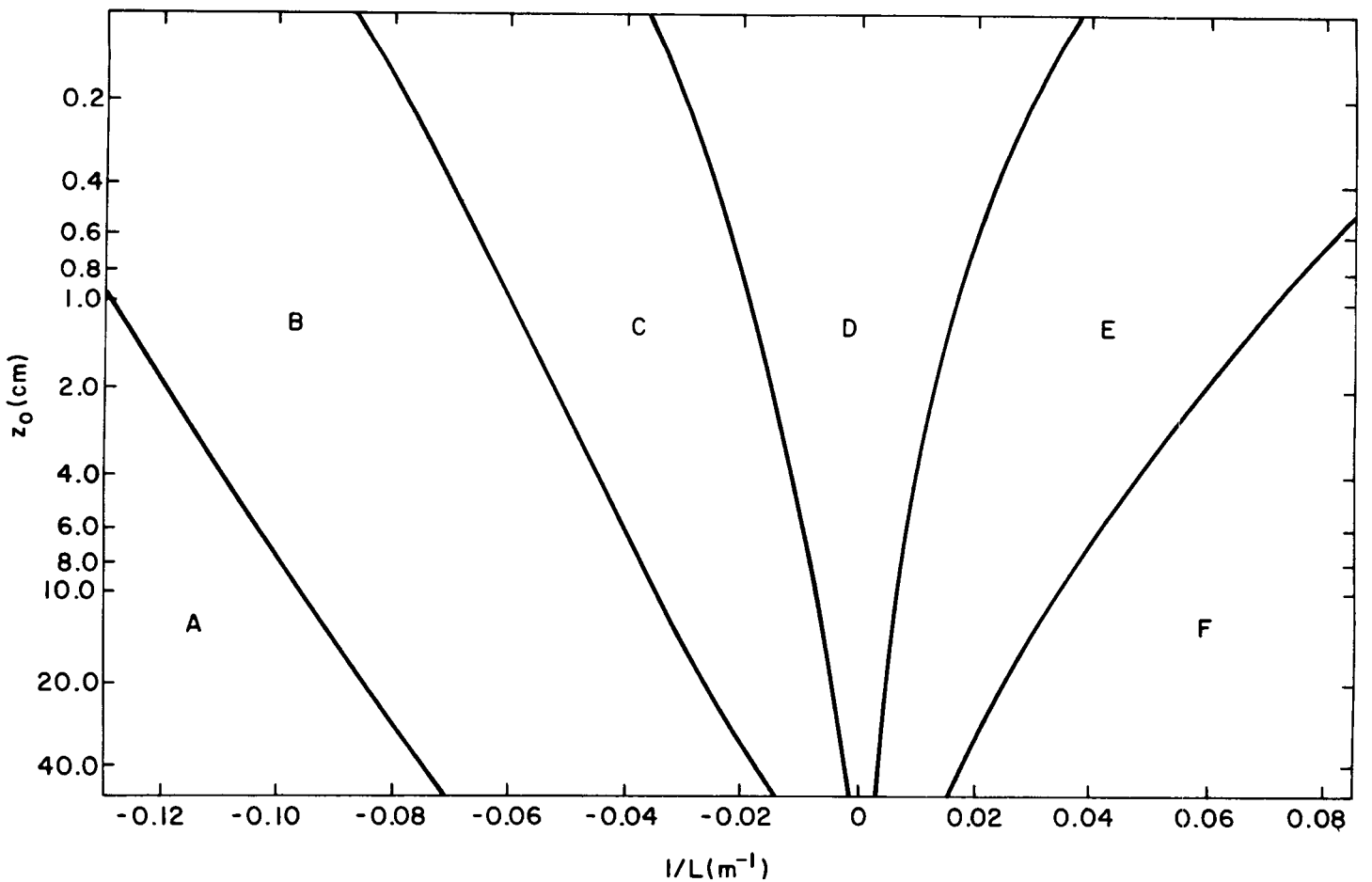

Figure 9. Pasquill class as function of $\frac{1}{L_o}$ and z_o.

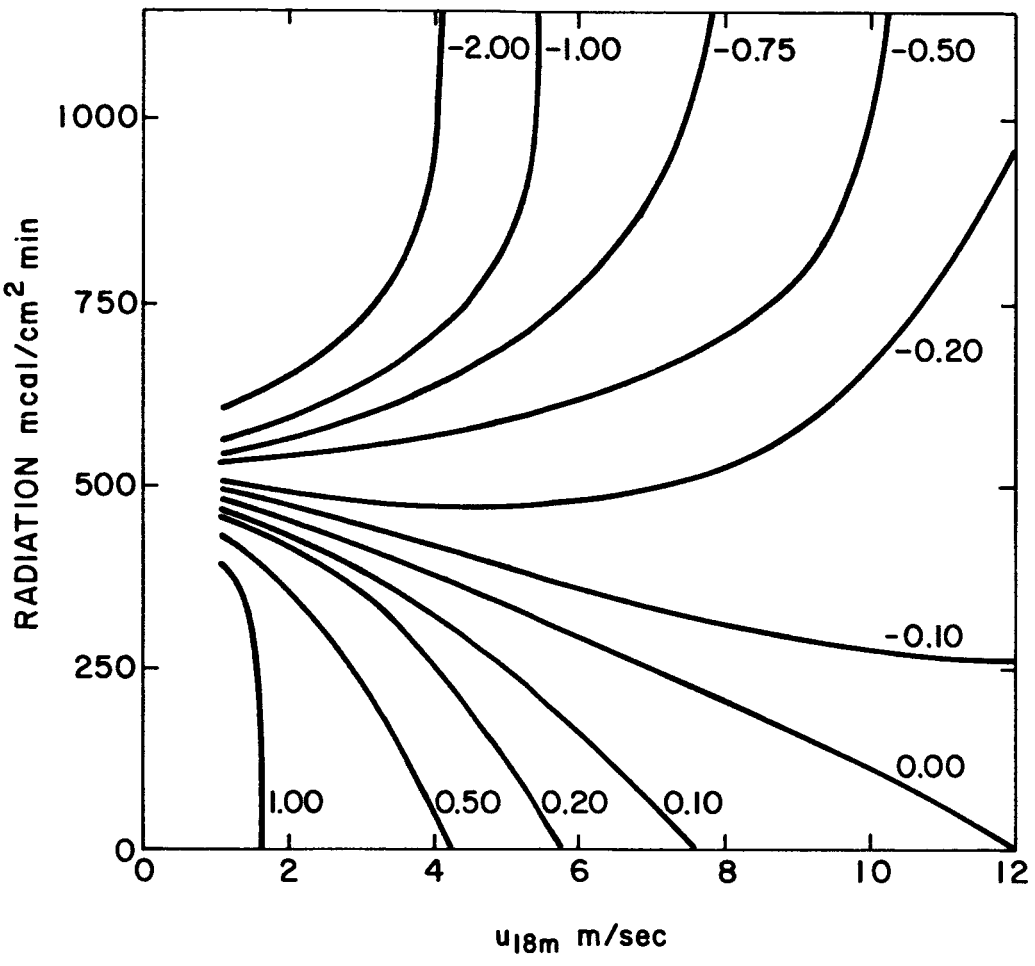

Figure 10. Richardson number as function of wind at 18 m and insolation.

Table 2. Relation of Pasquill stability classes to weather conditions

A - Extremely unstable conditions
B - Moderately unstable conditions
C - Slightly unstable conditions
D - Neutral conditions*
E - Slightly stable conditions
F - Moderately stable conditions

Surface Wind speed, m/sec	Daytime Insolation			Nighttime conditions	
	Strong	Moderate	Slight	Thin overcast or $\geq$ 4/8 Cloudiness**	$\leq$ 3/8 Cloudiness
<2	A	A-B	B		
2	A-B	B	C	E	F
4	B	B-C	C	D	E
6	C	C-D	D	D	D
>6	C	D	D	D	D

*Applicable to heavy overcast, day or night.

**The degree of cloudiness is defined as that fraction of the sky above the local apparent horizon which is covered by clouds.

Fortunately, u_{*_o} as determined from wind, roughness and stability is not very sensitive to the exact value of L_o, so that this quantity has to be known only approximately, and either of the last simple techniques to estimate it should be sufficient. The friction velocity is most sensitive to errors in wind speed, and, to a somewhat smaller extent, to errors in the roughness length.

The surface friction velocity is evaluated from the theory of the low-level wind profile, equation (15), given the wind near the ground z_o and L_o. We write (15) in the form:

$$u_{*o} = \frac{k\,u}{\ln z/z_o - \psi\,(z/L_o)} \tag{23}$$

As before, we adopt Paulson's form for $\psi(z/L_o)$ in unstable air (16). In stable air, as before

$$\psi\,(\frac{z}{L_o}) = -\,5\,\frac{z}{L_o} \tag{24}$$

Table 3 summarizes the friction velocities computed from (23) and (16) for all one-hour runs analyzed so far, along with other relevant statistics for each run. It is almost certain that local friction velocities estimated from (23) are more reliable than those that can be obtained from large-scale variables, including geostrophic wind. It is therefore recommended that, whenever possible, (23) be used for this purpose, given surface wind reports from hourly sequences.

Table 3. Friction velocities and other relevant statistics for each analyzed run at Cape Kennedy

Run No.	Wind Direction	Average Speed	Date	GMT Time On	GMT Time Off	Ri	z_o	u_{*_o}
001	346°		13 Feb	16:04	17:43			
013	10°	6.7	16 Mar	14:33	16:02	-.04	.29	1.21
020	320°	2.9	24 Mar	15:52	16:21	-.83	.44	
029	85°		30 Mar	13:26	14:14	+.14		
030	70°	4.4	31 Mar	13:33	14:33	-.16	.31	.97
057	105°	4.9	13 Apr	13:53	14:39	-.18	.35	.92
067	55°	3.3	20 Apr	17:59	18:40	-.32	.28	.80
070	130°	3.2	21 Apr	17:15	17:58	-.39	.41	
072	42°	2.8	25 Apr	15:09	15:31	-.56	.27	
075	155°	4.0	25 Apr	16:06	16:37	-.20	.59	.73
078	285°	4.2	27 Apr	18:52	19:22	-.04	.73	.78
080	289°	9.7	28 Apr	19:35	20:05	-.09	.72	
082	5°	4.2	28 Apr	15:38	16:08	-.12	.31	.91
086	242°	1.5	3 May	12:20	13:16	-.28	.52	.47
091	275°	4.0	8 May	17:42	18:42	-.17	.72	.78
095	170°	5.0	11 May	13:10	13:39	-.05	.68	
096	165°	4.5	11 May	16:30	17:30	-.19	.66	
098	25°	3.5	17 May	17:15	18:05	-.30	.28	.65
101	105°	2.6	19 May	16:11	17:11	-.23	.35	.42
104	173°	4.9	22 May	17:10	18:08	-.13	.69	
107	200°		23 May	18:06	18:36	+.08	.79	.49
110	325°	2.9	24 May	16:15	16:45	-.57	.47	
116	52°		1 June	14:00	14:30		.27	
118	90°	3.4	1 June	17:36	18:06	-.33	.32	.51
121	335°	2.6	19 June	12:48	13:48	-1.01	.38	.53
124	57°	1.4	20 June	14:16	14:42	-1.44	.29	
127	130°	3.2	21 June	14:52	15:52	-.38	.41	
133	140°	2.8	6 July	12:39	13:44	-.14	.46	.51
136	165°	2.9	10 July	15:35	16:42	-.24	.66	
137	180°		11 July	11:47	12:34		.72	
138	95°	1.8	11 July	16:07	17:14	-2.36	.33	.57

Table 3 (continued)

Run No.	Wind Direction	Average Speed	Date	GMT Time On	GMT Time Off	Ri	z_o	u_{*_o}
139	136°	2.4	11 July	17:30	18:41	-.69	.44	.53
140	168°		12 July	11:44	12:54		.68	
141	40°	1.9	12 July	16:30	17:40	-2.32	.27	.52
142	210°		12 July	01:28	02:38	+.08	.75	.42
143	220°		12 July	03:29	04:38	+.11	.63	.28
144	220°		13 July	05:04	06:14	+.14	.63	.24
149	125°	2.3	17 July	16:45	17:45	-.60	.39	.59
150	125°	2.3	17 July	18:09	18:40	-.36	.39	
151	90°		18 July	16:06	17:15	-9.75	.32	.50
152	60°		18 July	17:15	17:45		.29	
153	173°	1.4	19 July	15:00	16:00	-.81	.69	
154	90°	1.4	20 July	13:15	13:45	-.65	.32	
155	180°	2.1	24 July	16:36	17:36	-.31	.72	.36
156	130°		25 July	13:09	14:03	+.02	.41	.20
159	190°	2.5	25 July	16:30	16:59	-.66	.77	.55
160	230°	2.0	26 July	14:40	15:09	-.92	.55	.51
162	180°	3.0	28 July	16:36	17:37	-.20	.72	.54
163	110°	1.8	1 Aug	16:35	17:35	-.33	.36	.42
164	355°		2 Aug	13:09	14:03		.33	
165	100°	3.6	3 Aug	14:30	15:30	-.21	.34	.58
167	120°	1.6	3 Aug	16:07	16:37	-.27	.38	.27
170	130°		8 Aug	17:14	17:45	-5.08	.41	.67
172	120°	2.2	9 Aug	19:19	19:48	-.78	.38	.65
173	200°	2.0	10 Aug	14:16	14:46	-1.13	.79	
174	235°	1.4	10 Aug	17:16	17:46	-.68	.53	.25
176	115°	1.6	17 Aug	13:15	14:14	-1.08	.37	.38
179	130°		22 Aug	08:40	09:40		.41	
182	78°	2.8	24 Aug	16:29	17:29	-.46	.32	.58
183	60°	2.2	25 Aug	12:39	13:39	-.39	.29	.45
184	116°		29 Aug	00:15	01:15		.37	

Table 3 (continued)

Run No.	Wind Direction	Average Speed	Date	GMT Time On	GMT Time Off	Ri	z_o	u_{*o}
185	71°		29 Aug	01:16	01:45		.31	
187	36°		30 Aug	02:15	03:15		.27	
188	320°		30 Aug	03:13	03:44		.45	
189	340°	2.4	8 Sept	13:20	14:19	-.85	.36	.76
190	90°		12 Sept	12:46	13:46			
192	40°		12 Sept	14:17	14:37		.27	
193	90°		13 Sept	15:19	16:19		.32	
196	21°	2.9	14 Sept	20:11	21:10	-.44	.28	.66
197	21°	3.6	14 Sept	21:11	21:41	-.04	.28	
198	24°		15 Sept	21:41	21:57		.28	
199	358°	2.2	18 Sept	17:26	18:26	-.63	.32	
202	352°	3.0	19 Sept	18:51	19:20	-.41	.34	
204	50°		21 Sept	15:36	16:06		.27	
205	73°	1.6	21 Sept	18:04	18:19	-1.37	.31	
207	240°		22 Sept	16:21	17:15			
214	200°		28 Sept	17:08	18:08			
216	40°		2 Oct	15:36	16:37			
225	246°		10 Oct	00:00	01:00			
230	355°		12 Oct	13:44	14:44			
231	100°		16 Oct	16:30	17:30			
235	290°		18 Oct	15:04	16:04			
236	350°		19 Oct	16:00	16:45			
237	075°		23 Oct	14:49	15:49			
299	216°	6.0	23 Jan	16:27	17:12	-.067	.69	.78
302	264°	8.4	24 Jan	15:01	16:01		.65	
305	339°	8.5	26 Jan	16:42	17:42	-0.091	.36	.92
306	343°	9.0	26 Jan	17:42	18:11	-0.180	.36	1.03
307	215°	1.4	30 Jan	18:59	19:59		.69	
308	289°	10.1	6 Feb	18:27	19:27	-0.061	.72	1.32
309	303°	5.7	7 Feb	16:50	17:37	-0.598	.63	.88
310	298°	10.0	8 Feb	14:15	15:14	-0.165	.64	1.34
316	340°	4.4	14 Feb	15:06	16:06	-7.628	.36	1.02

Table 3 (continued)

Run No.	Wind Direction	Average Speed	Date	GMT Time On	GMT Time Off	Ri	z_o	u_{*o}
318	205°	5.6	23 Feb	17:50	18:50		.77	
319	322°	4.8	26 Feb	15:29	16:29	-2.542		
323		7.7	27 Feb	16:59	17:59	-0.236		
326	147°	4.3	28 Feb	17:59	18:29	-0.325		
327	211°	11.7	29 Feb	14:30	15:29	0.003	.75	1.47
330	270°	9.0	29 Feb	18:55	19:09		.70	
332	316°	7.2	1 Mar	17:10	18:10	-0.281	.49	.93
335	328°	4.5	6 Mar	15:59	16:59	-0.346	.40	.55
337	293°	9.3	7 Mar	18:09	18:40	-0.419	.72	1.44
338	76°	3.2	8 Mar	13:14	14:14	-1.053	.31	.42
341	202°	10.2	12 Mar	18:35	19:35	-0.060	.79	1.37
342	216°	7.9	12 Mar	19:35	19:51		.69	
345	290°	7.3	13 Mar	19:42	20:43	-0.037	.72	.94
350	74°	5.1	15 Mar	14:44	15:45	0.038	.31	.48
351	73°	7.4	15 Mar	16:59	17:28	-0.689	.31	.92
355	87°	3.9	20 Mar			-0.587	.32	.48
359	160°	9.0	22 Mar	16:59	17:59	-0.123	.64	1.18
361	161°	8.7	22 Mar	19:07	19:35	-0.092	.64	1.12
364	78°	6.1	27 Mar	14:55	15:55	-0.476	.32	.72
365	95°	5.0	28 Mar	14:05	14:31	-2.344	.33	.78
366	90°	6.1	28 Mar	16:45	17:45	-0.496	.32	.73
367	107°	2.3	29 Mar	15:09	15:40	-3.387	.35	.40
369	239°	3.3	1 Apr	14:45	16:45	0.070	.52	.32
370	98°	6.6	2 Apr	22:00	22:28	0.076	.34	.58
380		4.7	3 Apr	22:09	23:14	0.009		
381	155°	5.7	5 Apr	01:15	01:50	0.069	.68	.60
383	140°	2.8	4 Apr	07:45	08:45	0.215	.46	
384	149°	4.4	4 Apr	11:50	12:20		.55	
389	151°	6.6	4 Apr	23:10	24:10	0.081	.55	.63
394		6.2	6 Apr	02:00	02:43	0.032		
406	69°	4.4	7 Apr	20:06	20:37	-0.545	.31	.53
411	15°	7.6	12 Apr	00:50	01:14	0.086	.29	.63

Table 3 (continued)

Run No.	Wind Direction	Average Speed	Date	GMT Time ON	GMT Time Off	Ri	z_o	u_{*o}
414	151°	3.9	23 Apr	01:15	01:59	0.087	.55	.37
415	253°	6.7	24 Apr	20:27	21:01	0.001	.57	.71
445	94°	9.6	7 May	18:59	19:14	-0.017	.32	.97
447	88°	6.7	8 May	02:11	02:36	0.041	.32	.63
449	63°	5.0	9 May	22:29	23:04	-0.088	.29	
455	204°	3.5	12 May	14:45	15:04	0.063	.78	.37
457		1.8	15 May	02:22	02:52			
477	125°	5.4	3 June	20:20	20:59	-0.115	.39	.61
478	112°	6.5	4 June	01:33	02:02	0.003	.36	.66
480	70°	7.2	4 June	14:52	15:11	0.004	.31	.71
481	87°	7.1	4 June	15:30	17:29	0.038	.32	.67
487	14°	16.8	5 June	18:56	19:32		.29	
490	4°	11.3	6 June	00:54	02:22		.32	
491	8°	8.3	6 June	02:40	03:44	-0.004	.31	.82
515	89°	6.0	16 June	17:00	17:59	-0.284	.32	.68
521	105°	6.5	18 June	23:08	23:58	-0.073	.35	.69
522	175°	3.7	19 June	20:30	20:59	0.134	.70	.28
524	179°	3.6	20 June	00:01	00:46	0.113	.72	.32
526	305°	5.6	20 June	16:07	16:18	-0.356	.58	.78
529	337°	6.0	20 June	20:25	20:55	-0.081	.37	.64
536	161°	2.9	25 June	03:20	03:47	0.096	.64	.28
537	292°	6.8	25 June	20:04	20:51		.72	
539	212°	4.3	25 June	23:46	24:36	0.092	.75	.43
546	237°	5.4	27 June	20:51	21:50	0.034	.52	.58
547	297°	1.8	27 June	22:05	22:49	0.050	.64	.20
548	276°	3.0	28 June	16:37	16:57	-0.690	.74	.51
549	276°	2.4	28 June	19:00	20:00		.74	
551	36°	2.8	29 June	20:00	20:21	-8.497	.27	.60
554	85°	3.8	30 June	14:33	14:50	-1.631	.32	.55
555	73°	4.6	30 June	18:32	18:46	-1.479	.31	.64
559	138°	5.6	4 July	00:39	01:39	0.288	.46	

Table 3 (continued)

Run No.	Wind Direction	Average Speed	Date	GMT Time On	GMT Time Off	Ri	z_o	u_{*o}
565	227°	4.3	9 July	21:47	22:16	0.000	.55	.49
567	167°	4.4	10 July	01:12	01:37	0.016	.68	.52
610	105°	4.1	20 Sept	14:51	15:51	-1.355	.35	.59
614	67°	2.8	27 Sept	01:36	02:35	0.069	.31	.24
618	56°	8.7	5 Oct	18:20	19:20	-0.326	.29	.97
619	73°	5.2	6 Oct	12:40	13:08		.31	
625	37°	8.2	14 Oct	15:59	16:06		.27	
627	102°	7.9	15 Oct	23:05	23:50		.34	
631	130°	8.0	18 Oct	00:00	00:16		.41	
633	166°	10.1	19 Oct	06:45	07:45		.68	
640	311°	4.3	30 Oct	03:25	04:24		.53	
641	83°	2.4	2 Nov	02:55	03:52		.32	
642	150°	7.1	9 Nov	18:53	19:22		.55	
647	165°	3.0	3 Dec	01:55	02:54		.66	
648	217°	5.1	3 Dec	15:40	16:09		.63	
649	301°	7.0	4 Dec	13:10	13:37		.64	

IV. DETERMINATION OF PREDICTANDS FROM z_o, u_{*_o}, AND L_o

4.1 Estimation of Mean Wind

Wind profiles were discussed in detail in Chapter II. Briefly, the usual logarithmic expressions appear to be valid in neutral air up to the top of the tower, 150 m; further, the corrections in unstable air developed for the surface layer supply good fits at high levels as well. Some systematic exceptions at Kennedy occurred, however, for example, with westerly winds, the winds at 30 m and 60 m exceeded those expected from the simple profile theory. As previously mentioned, the explanation for this apparent anomaly may perhaps be found in the stretch of forest, about 200 m to 400 m west of the tower.

Once u_{*_o} and L_o have been determined by methods suggested in Chapters III or V, then (15) and (16) may be used to estimate the wind profile. However, simpler procedures can sometimes be used. For example, a frequent practical problem is that wind, and perhaps temperatures, or radiation, are given near the surface. The wind at one or more higher levels must be estimated. This problem can be handled by dividing (12) at a higher level (subscript 2) by (12) at a low level (subscript 1). The result is

$$u_2 = u_1 \frac{\ln\left(\frac{z_2 e^{-\psi_2}}{z_o}\right)}{\ln\left(\frac{z_1 e^{-\psi_1}}{z_o}\right)} \qquad (24)$$

The roughness length is given, at Kennedy, from Figure 5. At other locations, the roughness lengths are assumed known, at least approximately.

Equation (16) or Table 1 gives ψ in unstable air, and in slightly stable air, (Ri < .10). For more stable air, (24) is of doubtful value; the more stable the air, the less winds near the surface are coupled with winds higher up, so that winds at 100 m or so cannot be estimated from conditions close to the ground.

Engineers often estimate high-level winds from power laws, which fit profiles reasonably well:

$$\frac{u_2}{u_1} = \left(\frac{z_2}{z_1}\right)^p \tag{25}$$

The best fit of such power laws to profiles is obtained if the exponent p is computed from:

$$p = \frac{\phi}{\ln \bar{z}/z_o - \psi} \tag{26}$$

Here, $\bar{z}$ is the geometric mean height between z_1 and z_2. ϕ is the usual normalized wind shear and is tabulated above in Table 1. A nomogram for p as function of $\bar{z}/z_o$ and $\bar{z}/L_o$ is Figure 11.

Usually, "random" errors in the high-level winds are larger than errors produced by slight errors in z_o or L.

4.2 Estimation of Variances

According to Report 2 and Monin-Obukhov theory, the standard deviations of the velocity components are well correlated with the friction velocity; further, the ratio of standard deviations and friction velocity should be dependent on z/L_o.

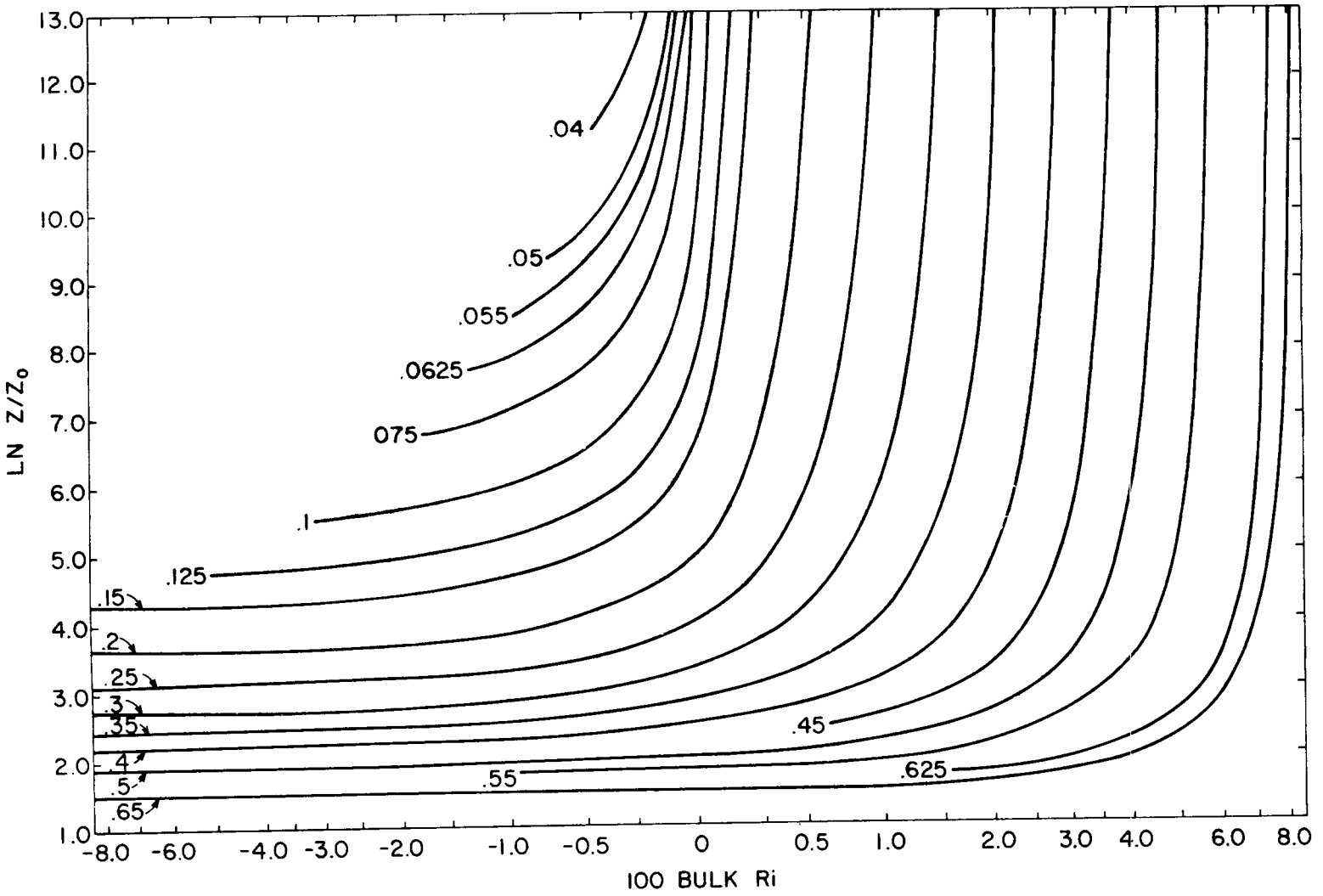

Figure 11. Nomogram for wind profile exponent as function of z/z_o and bulk Richardson number.

Since friction velocities have been revised in accordance with the revised roughness lengths, Figures 12 to 15 show new relationships between the standard deviations and the friction velocities on the one hand, and between standard deviation-friction velocity ratios and z/L, on the other. The best estimate for σ_u/u_* in neutral air is now 1.6, and that for σ_v/u_*, also 1.6. These ratios are smaller than those found on the average (see Lumley and Panofsky, 1964). However, they are nearly the same as at Brookhaven, which is located, like Kennedy, in a generally flat countryside. It is likely that these ratios are not universal, but depend also on a mesoscale roughness which controls the low frequency portion of the spectrum of the horizontal velocity components. If the mesoscale variations are pronounced, for example, the ratio σ_u/u_* sometimes exceeds 3. The correlation coefficients between σ_u and σ_v with u_* are quite high, being 0.87 for σ_u and 0.45 for σ_v. This suggests that σ_u, and to a smaller extent, σ_v, can be estimated accurately from u_*, provided that u_* can be obtained without systematic error, at least at Kennedy, once u_* is well estimated.

In contrast to earlier results, Figures 13 and 15 show no systematic variation of σ_u/u_* and σ_v/u_* with z/L. As to other locations, there are no constant relations between these ratios and stability.

In spite of the argument that σ_u/u_* and σ_v/u_* really could be as low as the observed ratios of 1.6, there is even better evidence that the true ratios should be about 50% larger. The argument for this will be discussed more fully in Section 4.3 In that case, the ratios are more nearly equal to those recommended by Lumley and Panofsky (1964). If this is correct, either the assumed roughness lengths are too large or the measured standard deviations are too small. Since

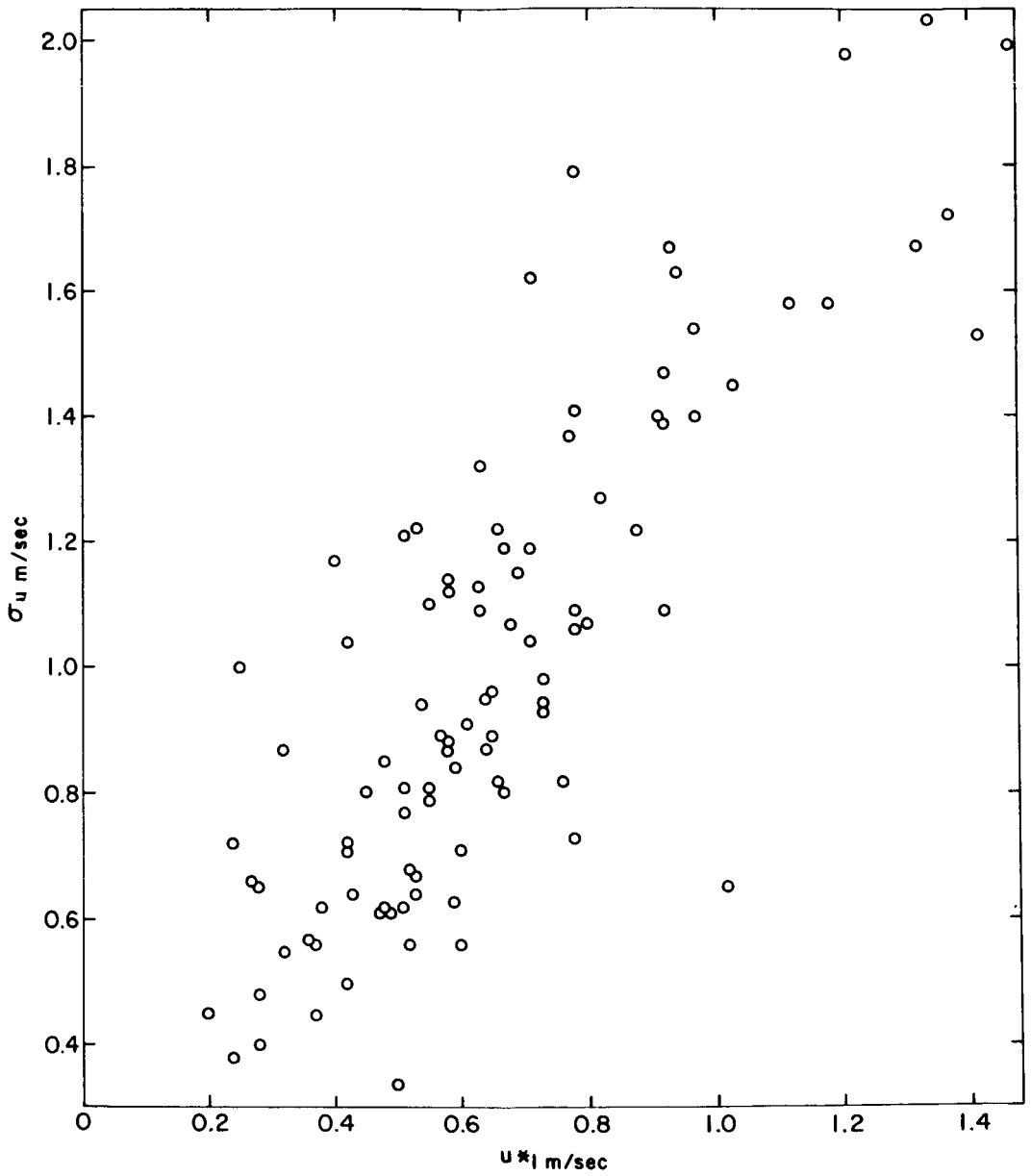

Figure 12. Observed values of σ_u vs u_*, m sec^{-1}, at Cape Kennedy.

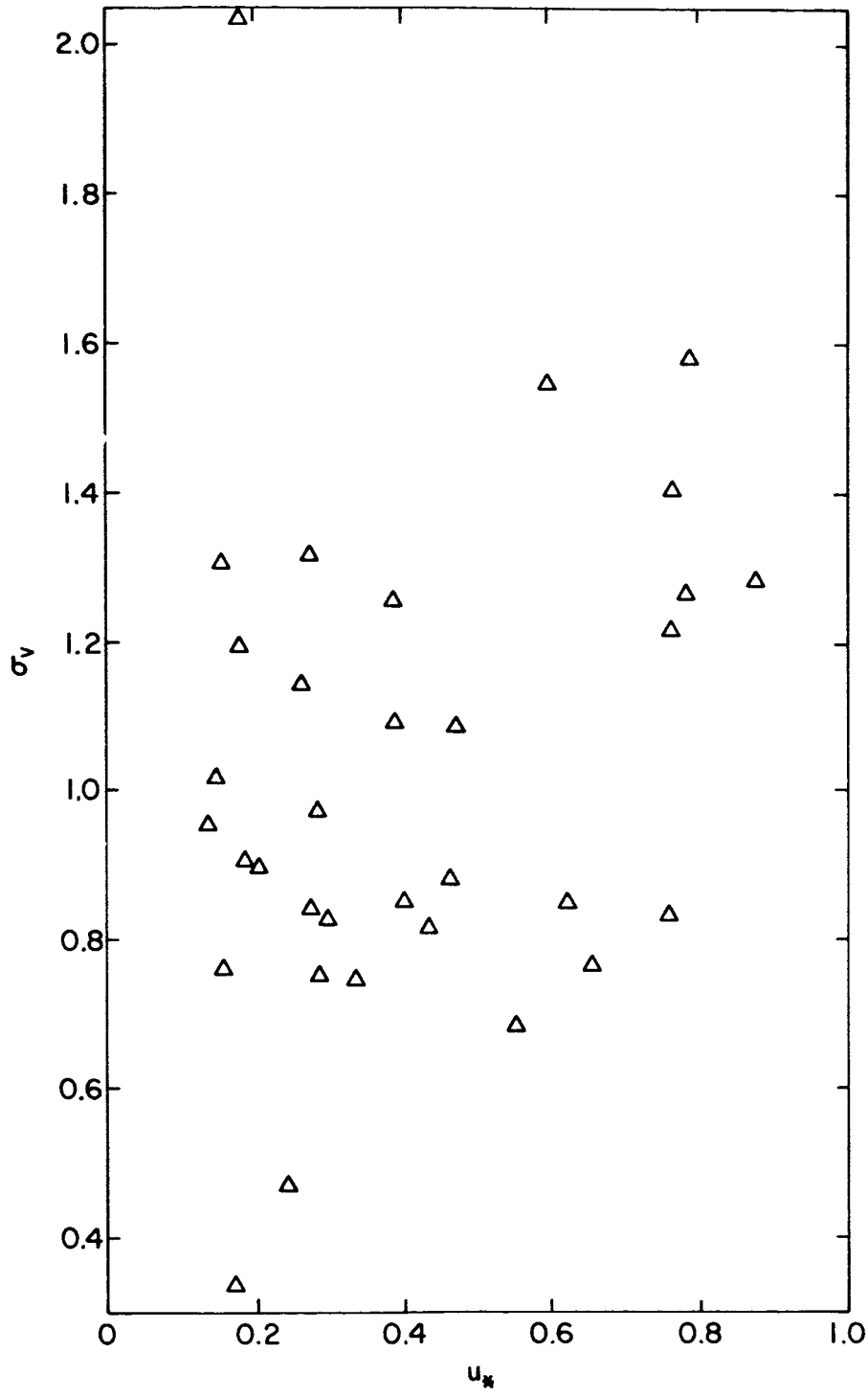

Figure 13. Observed values of σ_v vs u_*, m sec^{-1}, at Cape Kennedy.

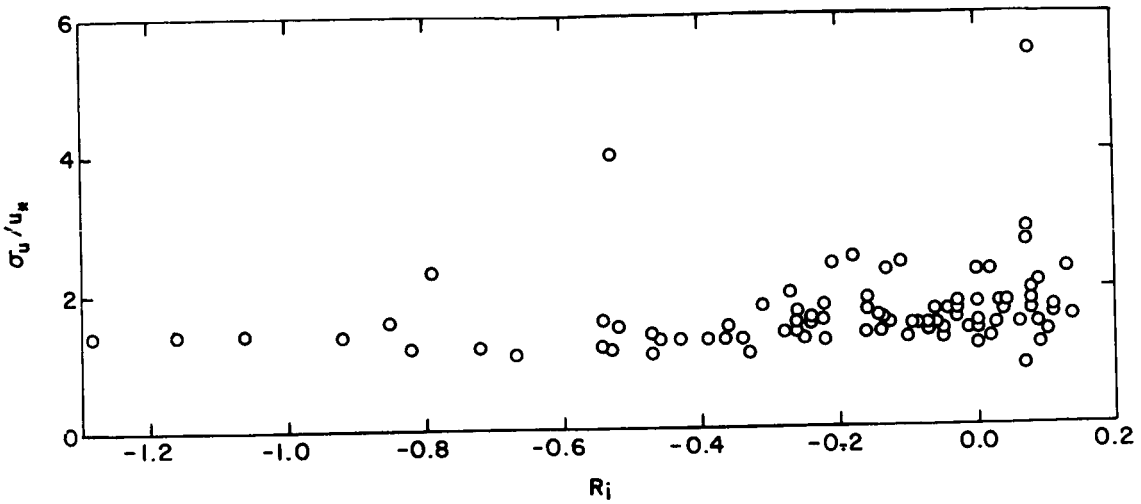

Figure 14. Observed ratios σ_u/u_* vs Ri.

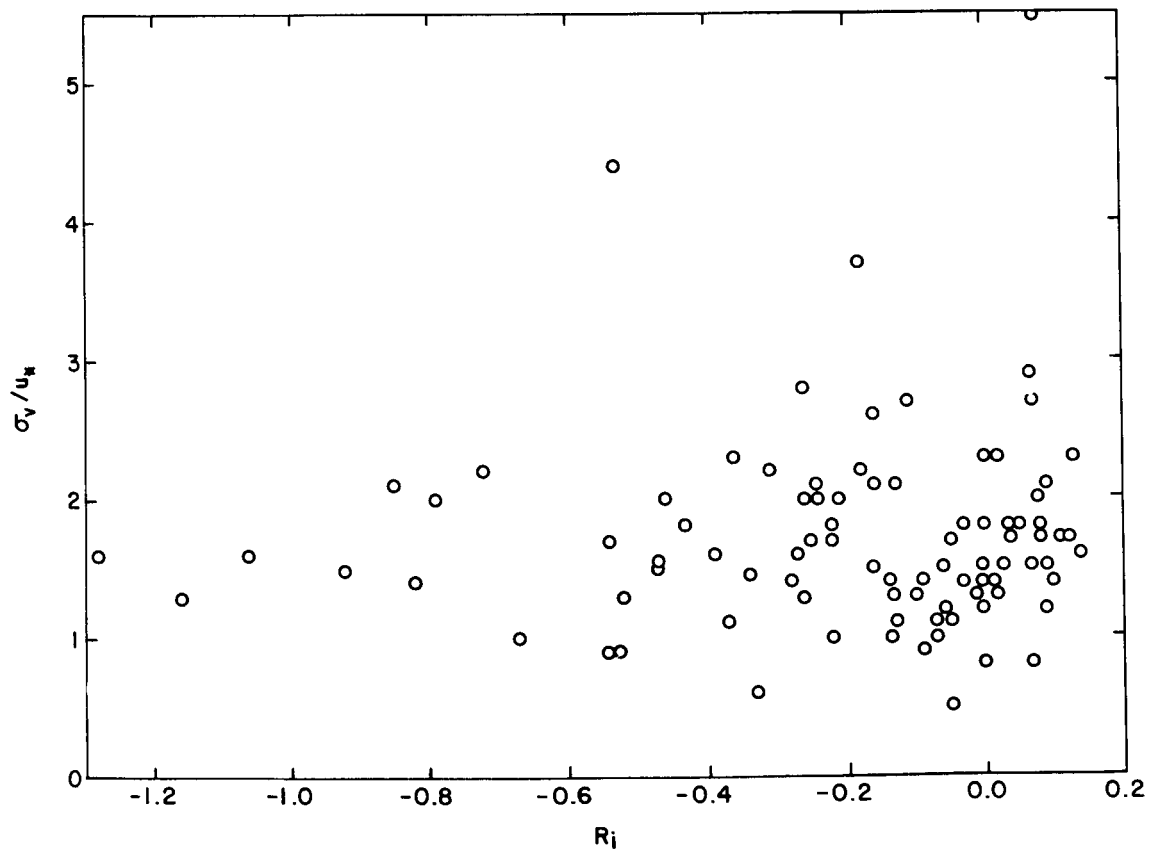

Figure 15. Observed ratios σ_v/u_* vs Ri.

the roughness lengths depend critically on the vertical wind shears, this means that the statistical fluctuations are too small for the wind shears. There is no objective way to determine whether the wind shears are too large or the fluctuations too small. We will make the hypothesis here that the wind shears have no systematic errors, but that all measured fluctuation statistics are about 2/3 of their true value, perhaps due to instrumental imperfections or problems with the recorder. Hence, for estimations of σ_u and σ_v, we will assume that $\sigma_u \sim 2.5\ u_{*o}$ and $\sigma_v \sim 2.2\ u_{*o}$ as suggested by Lumley and Panofsky. Further, these factors will be assumed to be relatively independent of stability. As mentioned before, we recommend that u_{*o} be estimated from (23) as function of z_o, L_o and wind at a low level.

Report 2 also showed a relation between the difference of high-level and low-level standard deviations σ_u and the wind at 18 m, in the sense that the variance decreased most rapidly in strongest winds; for example, there is no change when the wind is 3 m/sec, and the variance decreases by 7 $m^2\ sec^{-2}$ from 18 m to 150 m with a wind of 8 m/sec. This result has not been explained but the relation is reproduced as Figures 16, and Figure 17 shows the analogous relation for σ_v.

Theoretically, one might expect the decrease to be largest in the most stable air; in unstable air the increase of $-z/L$ with height should diminish or even reverse this tendency. Table 4 shows that fractional change of average standard deviation with height (relative to unity at 18 m).

According to Table 4, the decrease of the longitudinal standard deviations is indeed largest for the most stable air; further, in unstable air, the decreases for longitudinal and lateral standard deviations are about the same;

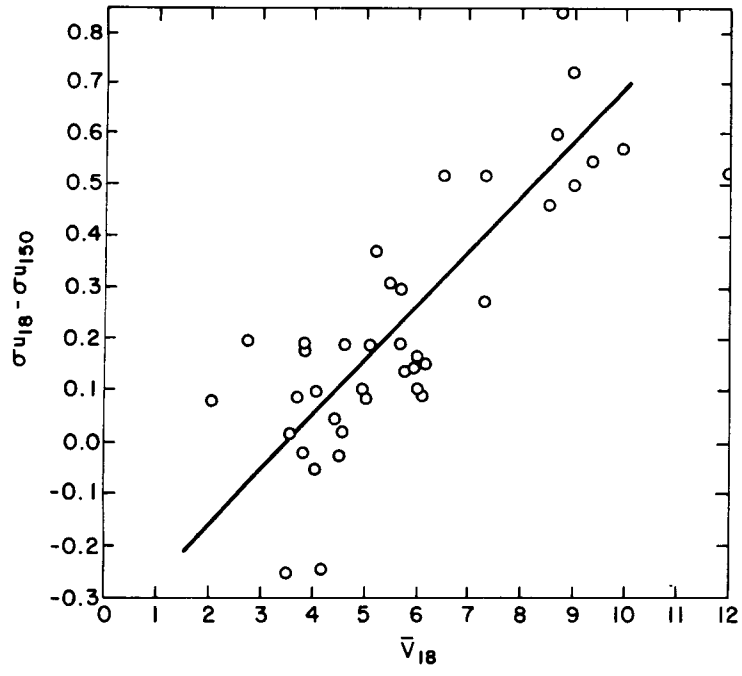

Figure 16. σ_u at 18 m minus σ_u at 150 m as function of wind speed at 18 m.

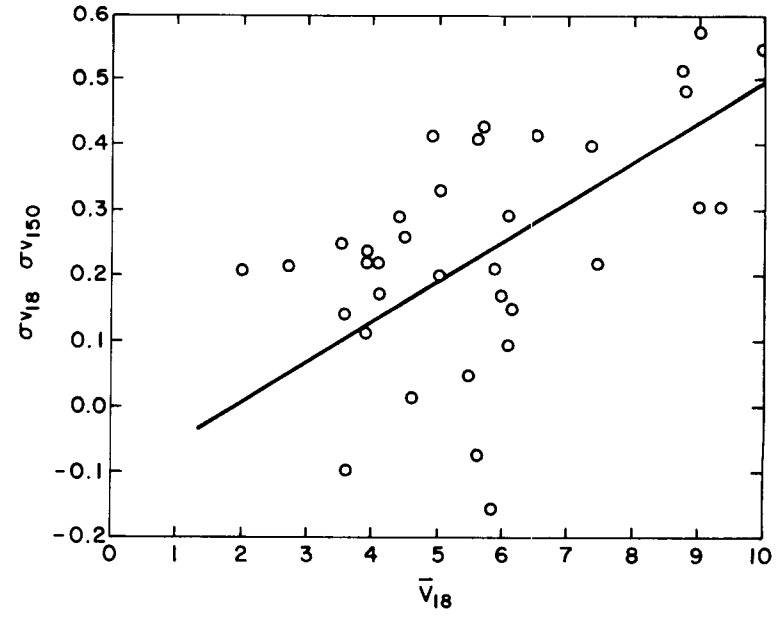

Figure 17. σ_v at 18 m minus σ_v at 150 m, as function of wind speed at 18 m.

Table 4. Vertical variation of average standard deviation of u and v for different stability groups

Height, m	18	30	60	90	120	150
			Ri > -.1			
σ_u	1.00	1.01	.95	.83	.80	.77
σ_v	1.00	1.04	1.00	1.02	1.03	1.05
			$-0.20 \leq Ri \leq -.1$			
σ_u	1.00	1.01	.92	.84	.81	.78
σ_v	1.00	1.01	.97	.86	.86	.86
			Ri < -2.0			
σ_u	1.00	.98	.94	.90	.87	.86
σ_v	1.00	1.04	.94	.90	.84	.83

however, in the near-neutral class, average lateral standard deivations actually increase upwards, though not significantly. In fact, upward decreases are slightly more common in this category than increases. This points up the tremendous variability of the change of these statistics with height, so that the systematic changes shown in the table do not reflect well the behavior in individual cases. All we can say with certainty is that the systematic change of the standard deviations is generally small, and that decreases exceed increases. Wind speed appears better related to the vertical change than Richardson number (Figures 16 and 17). But, since the relations of wind speed to changes of the σ's with height have not been explained it is probably best at present that we assume for estimation purposes that no significant vertical variation of the σ's exists.

4.3 Estimation of Spectra

Fichtl and McVehil (1970) have discussed spectra of lateral and longitudional velocity components at Cape Kennedy in some detail. For many applications to rocket problems, the inertial-subrange portion of the spectra is of special importance, and will be discussed here. For horizontal wind components, this range extends from wavelengths several times the height to wavelengths of 1 cm or less. The exact range was discussed in detail in Report 1.

The equation for the spectra in the inertial subrange is:

$$S(k) = a\varepsilon^{2/3} k^{-5/3} \tag{27}$$

Here, "a" represents universal constants, which are about 0.5 for longitudinal components and 0.67 for lateral components, if the wave number k is measured in radians per unit length. Hence, the problem of estimation of spectra in the subrange reduces the problem of estimating the dissipation, ε.

In general, the dissipation can be written in terms of the nondimensional function, ϕ_ε:

$$\varepsilon = \frac{u_{*o}^3}{0.4z} \phi_\varepsilon \tag{28}$$

Panofsky, in Report 1, has suggested that, for practical purposes, at 30 m and above, vertical divergence of turbulent energy flux can be neglected, so that (neglecting the pressure term in the energy budget and assuming equilibrium)

$$\phi_\varepsilon = \phi - z/L_o \tag{29}$$

Fichtl and McVehil (1970) have suggested that, at 18 m and perhaps below, vertical flux divergence and buoyant energy reproduction cancel (see also Panofsky, 1962) so that

$$\phi_\varepsilon = \phi \tag{30}$$

The cancellation of divergence and buoyant production at low levels has recently been confirmed by Wyngaard and Cote (1971), but (30) has not. Wyngaard and Cote's conclusion is that the pressure term is important to the turbulent energy budget in unstable air. Nevertheless, (29) and (30) seem to explain well the ratio of energy dissipation estimates at different heights quite satisfactorily, as seen in Report 1, where ϕ was taken as $(1 - 18\ z/L_o)^{-1/4}$.

The problem of estimating ε at any level then reduces to estimating it at a low level, taken here as 30 m (where it is, according to (28) and (29))

$$\varepsilon_{30} = \frac{u_{*o}^3}{12}\left[\phi\left(\frac{30}{L_o}\right) - \frac{30}{L_o}\right] \tag{31}$$

Figure 18 compares $\sqrt[3]{\varepsilon_{30}}$ determined from observed lateral and longitudinal spectra with the corresponding estimates from (31), with u_{*o} taken from Table 3. Apparently the magnitude of the "observed" values of $\sqrt[3]{\varepsilon}$ is only about 2/3 of the "computed $\sqrt[3]{\varepsilon}$, on the average. The agreement is best for weak winds at 30 m and poorest for strong winds. This would be expected if

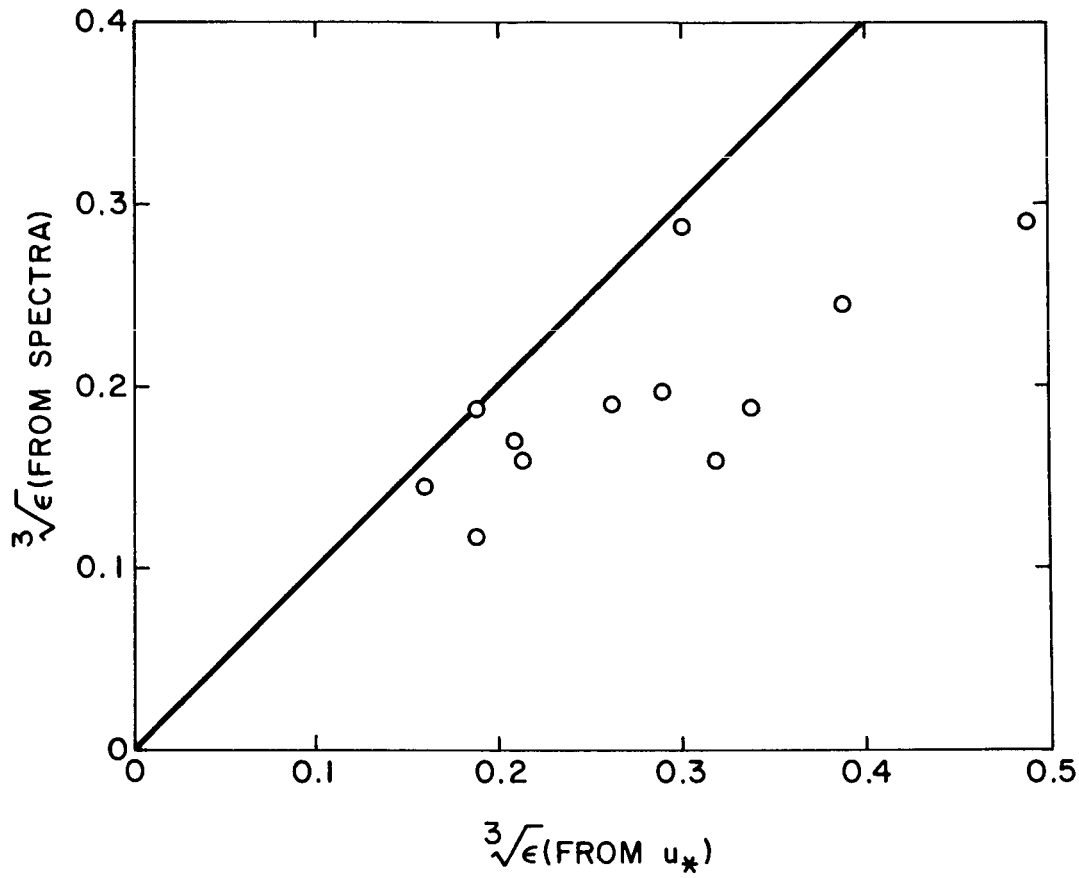

Figure 18. "Observed" $\sqrt[3]{\epsilon}$ vs $\sqrt[3]{\epsilon}$ estimated from surface stress, c.g.s. units.

the discrepancy was due to errors in the dissipation estimated from the spectra; the stronger the wind, the more these estimates depend on high frequencies, which would be most strongly damped if there was undue friction in the anemometer. The tentative assumption will then be made that the "computed" values of ε are better than "observed" values. This assumption is consistent with the assumption in past sections that "measured" standard deviations are too low. In other words, (31), with u_{*_o} determined from (23) and the roughness lengths of Figure 5 is assumed to result in the best estimates of ε at 30 m.

In Chapter VI, suggestions are made concerning the "best" procedure for obtaining u_{*_o} from geostrophic winds. However, such estimates are likely to be less accurate than those from (23), based on low-level winds, assumed roughness lengths and L_o determined from radiation and wind, as described in Chapter III.

There is at least one flaw in the preceding argument. If ε values estimated from the spectra measured at Kennedy are systematically too low, the error should decrease with increasing heights, as high frequencies become less important. Hence, observed ratios of dissipations at 120 m to those at 30 m may be too large. Equation (29) was based on this ratio and should be re-examined with more reliable estimates of ε from spectra.

Nevertheless, for the time being, it is still suggested that we can use (29) to estimate ε above 30 m:

$$\varepsilon = \varepsilon_{30} \left| \frac{(1 - 16 \frac{z}{L_o})^{-1/4} - \frac{z}{L_o}}{(1 - \frac{480}{L_o})^{-1/4} - \frac{30}{L_o}} \right| \frac{30 \text{ m}}{z}$$

4.4 Estimation of Cross Spectra in the Vertical

Cross spectra are usually characterized either by cospectra and quadrature spectra, or by coherence, Co, and slope, S, defined by

$$Co(n) = \frac{Cos^2(n) + Q^2(n)}{S_1 S_2} \tag{32}$$

and

$$S = \frac{u}{2\pi n \Delta z} \arctan \frac{Q(n)}{Cos(n)} \tag{33}$$

where Q is the quadrature spectrum and Cos the cospectrum at frequency n. Δz is the height interval and u the mean speed in Δz. In practice, slope and coherence seem to have simpler properties than cospectrum and quadrature spectrum. Therefore, the procedure recommended is to estimate coherence and slope first, and then estimate co- and quadrature spectra, or space-time correlation function by cosine transform (equation 2.1, Report 2).

As was first suggested by Davenport (1961), coherence can be well fitted by exponentials of the form:

$$Co(n) = e^{-a\Delta f} \tag{34}$$

Here, Δf is the nondimensional frequency, $n\Delta z/u$ and a is a "decay constant" which depends on Richardson number. Figures 19 and 20, reproduced from Report 2, show the relationship between decay constant and Richardson number at 23 m. The systematic difference between Kennedy and other sites is still unexplained, but believed to be due to random errors in the Kennedy data.

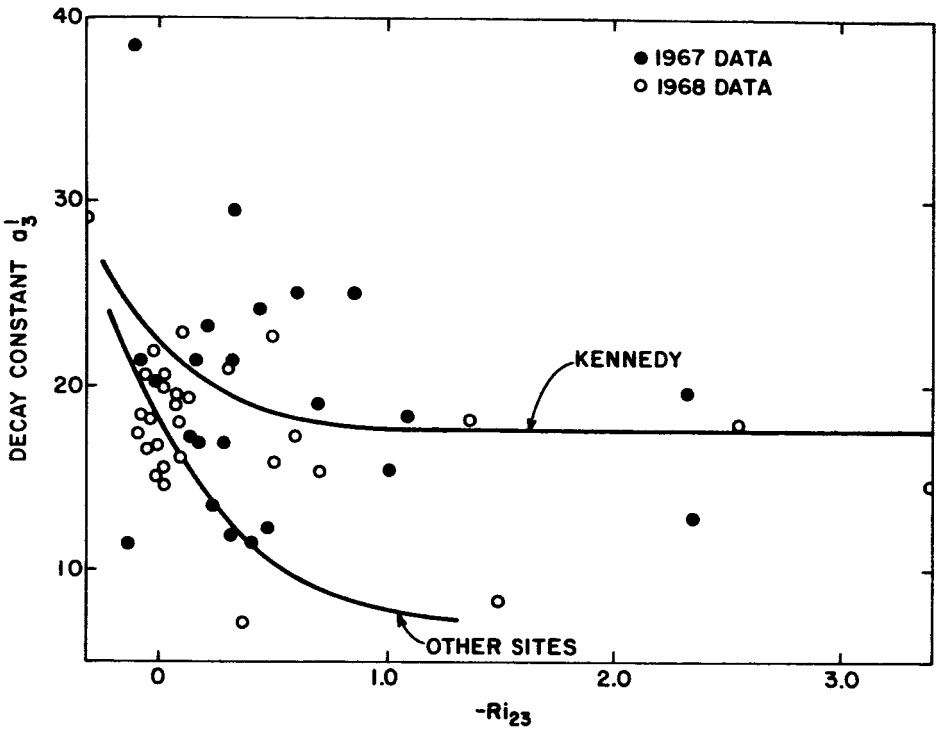

Figure 19. Decay constant for coherence of u as function of Ri at 23 m.

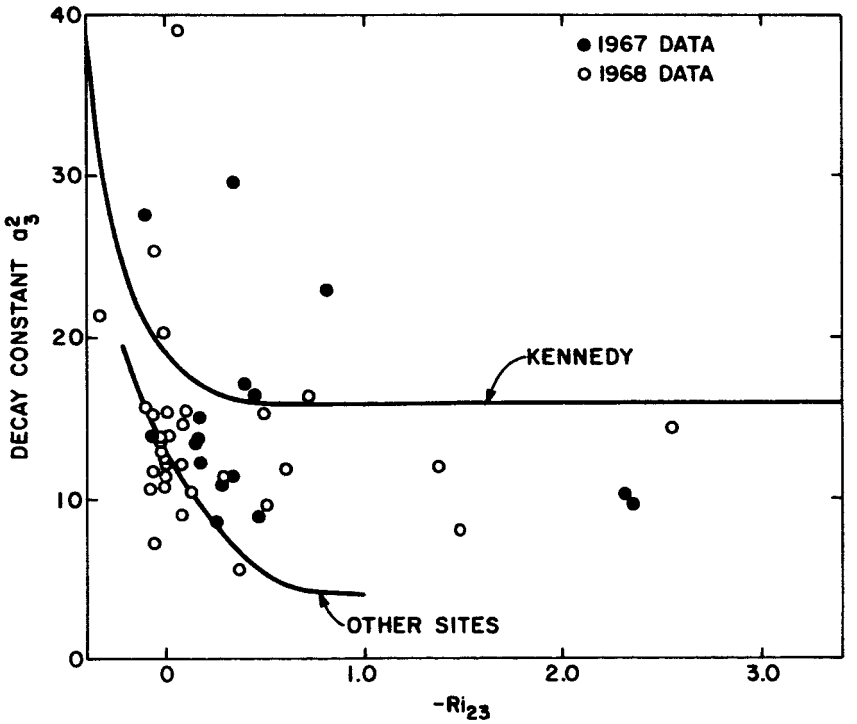

Figure 20. Decay constant for coherence of v, as function of Ri at 23 m.

Figures 21 and 22 reproduce the corresponding figures from Report 2 showing relationships between slopes and Richardson number; here the agreement between Kennedy and other sites is good. Also, slopes for the lateral components are about twice those of the longitudinal components.

The slopes are relatively constant up to 100 m, but average about 50 percent less between 120 m and 150 m; for details, see Report 2.

Since the writing of Report 2, considerable work has been done on decay constants for horizontal separations. The decay constants at right angles to the wind are about the same as the vertical constants. The longitudinal constants are much smaller and probably increase with increasing relative turbulent intensity.

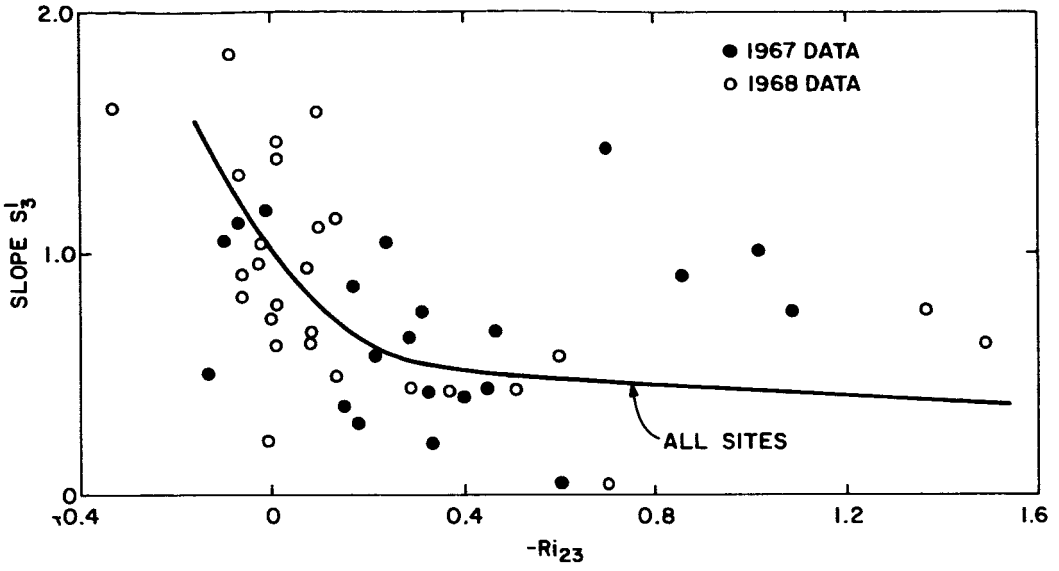

Figure 21. "Slope" of u vs Ri.

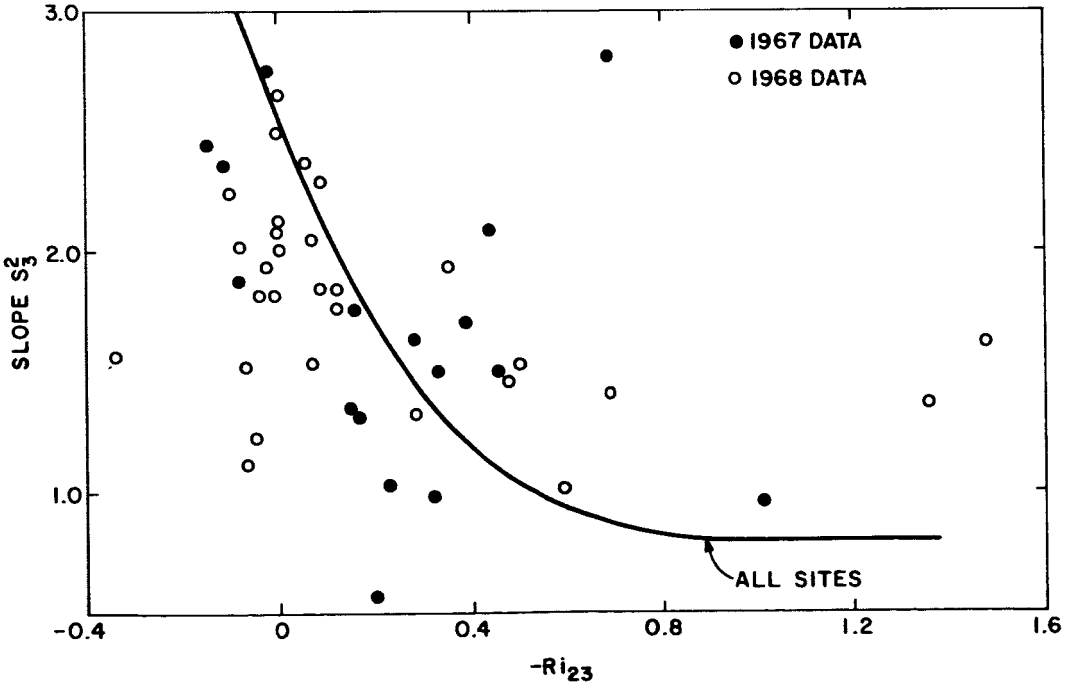

Figure 22. "Slope" of v vs Ri.

V. RELATIONS BETWEEN LARGE SCALE PARAMETERS AND u_{*_o}, L_o

5.1 Theory

It has been seen that the mean wind distribution in the surface layers, together with the distributions of a number of statistics of the turbulent flow, is determined by the parameters z_o, u_{*_o} and L_o. These quantities may be thought of as predictors of the mean wind and turbulence statistics, since the relationships between them are now established. However, u_{*_o} and L_o are not satisfactory for this use, since their determination by ordinary methods requires a knowledge of the predictands themselves. It is therefore required to find appropriate bases for estimating the values of u_{*_o} and L_o from larger scale variables, such as can be derived from synoptic data or from numerically calculated properties of the large scale flow.

The basis of such relationships has been laid in theoretical studies of the planetary boundary layer by many authors. An equation relating the geostrophic drag coefficient u_{*_o}/V_g to the surface Rossby number V_g/fz_o was first derived by Kazanski and Monin (1961) for neutral stratification, and was later broadened to diabatic boundary layers by Monin and Zilitinkevich (1967) using the semiempirical theory. Similar relationships have been derived more recently by Gill (1967), Csanady (1967), Blackadar and Tennekes (1967) and Blackadar (1969) using singular perturbation methods to match the flow in the surface (constant stress) layer to that of the outer layer which is dominated by the earth's rotation and buoyancy. The theoretical justification of these latter methods has been discussed in detail by Blackadar and Tennekes (1968).

In this section we review briefly the theoretical justification and the probable limitations of these relations as we now know them.

The flow within a neutral barotropic planetary boundary layer (PBL) is completely determined by the quantities z_o, u_{*o}, the Coriolis parameter, f, and the height z. Because the surface boundary condition requires the velocity to vanish at the lower surface, the flow close to the surface is dominated by the surface roughness z_o; this condition can be achieved only by scaling heights close to the surface by z_o. On the other hand, throughout the principal portion of the PBL the appropriate length scale for the wind distribution must be u_{*o}/f. This fact follows directly from the equations of motion and the necessity for the geostrophic departure to scale as u_{*o} (Blackadar and Tennekes, 1968). Accordingly, the principal dimensionless parameter is the ratio of the two length scales, u_{*o}/fz_o, which may be called the drag Rossby number. In addition to this number there exists the independent dimensionless ratio zf/u_{*o}, and it can be shown from Buckingham's theorem that all other dimensionless characteristics of the neutral PBL are functions of these two dimensionless ratios.

Normally, the drag Rossby number is very large, typically 10^4 to 10^6, and it is a reasonable hypothesis to treat the case when this parameter approaches infinity. In this case, the equations of motion demand that the scale velocity deficits $(u - u_g)/u_{*o}$ and $(v - v_g)/u_{*o}$ be universal functions of zf/u_{*o} only as long as $z \gg z_o$. It can further be shown that a necessary and sufficient condition for satisfying the boundary conditions is that the flow near the surface be logarithmic. Also, the logarithmic solution in the surface layers is compatible with the universal function of

the outer layer only if the Kazanski-Monin relationships are satisfied:

$$\frac{u_g}{u_{*o}} = \frac{1}{k}\left[\ln \frac{u_{*o}}{fz_o} - A\right] \tag{35}$$

and

$$\frac{v_g}{u_{*o}} = -\frac{B}{k} \tag{36}$$

where A and B are constants the values of which must be determined empirically or from more complete models of the flow. In these equations, the x-direction is parallel to the surface stress. The equations may be considered as implicit relations for calculating the values of u_{*o} and the surface wind-drift angle α when the direction and magnitude of the geostrophic wind are known.

Model studies of the flow in the PBL make it possible to relate the two constants A and B to a single disposable constant (Blackadar and Tennekes, 1968). When this constant is chosen so as to achieve the best fit of empirical data, it is found that A and B are about 0.0 and 4.5, respectively. The resulting wind distribution is rather similar to the classical Ekman spiral with a gradient wind level at a height zf/u_{*o} equal to about 0.25.

The argument for the universality of the functions $(u - u_g)/u_{*o}$ and $(v - v_g)/u_{*o}$, on which the neutral equations (35) and (36) depend, rests on the assumption that there are no relevant parameters other than u_{*o}, f, z_o, and z. Such ideal conditions seldom, if ever, prevail. We must, in

practice, be concerned with such matters as non-steady states, horizontal temperature gradients (baroclinicity), and diabatic vertical temperature gradients.

The effects of baroclinicity on the surface wind direction appear to be rather conspicuous, but as far as they affect u_{*_o} they are minor. This conclusion is based on the results of two models studied by Blackadar (1965a, b). The effect of vertical temperature gradients will be considered in two parts: (a) the effects of the presence of an inversion at some level h that effectively prevents the downward flux of momentum and heat from above, and (b) the effect of a heat source at the surface that results in the generation of convection by buoyant processes within the PBL.

It frequently happens that a stable layer above the surface is transformed by mechanical mixing into an adiabatic layer surmounted by an inversion, which must be considered to be impervious to the flux of momentum. If the inversion is high in comparision, say, to .25 u_{*_o}/f, its effect on the flow, and therefore on u_{*_o} is negligible, for the momentum flux at these levels would not be significantly changed by the presence of the inversion. We expect, therefore that h will be a significant parameter only when it is small compared to u_*/f. We shall study this case in detail. This conclusion is supported by Deardorff, who found by numerical simulation, values for A and B of 1.3 and 3.0 when $hf/u_* = 0.5$. These values are reasonably consistent with those found with other models where h is infinitely large.

Steady-state flow in the PBL is governed by the equations

$$f(v-v_g) + \frac{d}{dz}\left(\frac{\tau_x}{\rho}\right) = 0 \qquad (37)$$

$$-f(u-u_g) + \frac{d}{dz}\left(\frac{\tau_y}{\rho}\right) = 0$$

subject to the boundary conditions at the surface

$$u(z_o) = 0;\ v(z_o) = 0;\ \tau_x(z_o) = \rho u_{*o}^2;\ \tau_y(z_o) = 0 \qquad (38)$$

and to the condition that at height h the stress vanishes.

The presence of the variable h requires the definition of three independent dimensionless products, and we choose for these the following set

$$Z = \frac{zf}{u_{*o}},\ R = \frac{u_*}{fz_o},\ \text{and}\ Z_h = \frac{hf}{u_{*o}} \qquad (39)$$

As in the earlier theories, we assume that the flow is independent of z_o except in the immediate vicinity of the surface. Accordingly, the equations of motion suggest

$$\left(\frac{u - u_g}{u_{*o}}\right) = \hat{u}\ (Z,\ Z_h)$$
$$\left(\frac{v - v_g}{u_{*o}}\right) = \hat{v}\ (Z,\ Z_h) \qquad (40)$$

while in the surface layer, the surface boundary condition requires

$$\frac{u}{u_{*o}} = f_1\ (z/z_o) = f_1\ (ZR) \qquad (41)$$

and, because of the chosen direction of the x-axis

$$\frac{v}{u_{*o}} = 0 \qquad (42)$$

Since the geostrophic wind is considered to be independent of height, we have

$$\frac{u_g}{u_{*o}} = \hat{u}_g\ (R,Z_h) \qquad \frac{v_g}{u_{*o}} = \hat{v}_g\ (R,Z_g) \tag{43}$$

We now require that as R approaches infinity, the solutions for the two layers match each other in a layer the height of which is small compared to u_{*o}/f and h. Accordingly, we have, for such a layer,

$$f_1(ZR) \equiv \hat{u}_g(R,Z_h) + \hat{u}(Z,Z_h) \tag{44}$$

We may now proceed to differentiate this equation successively with respect to each of the three arguments Z_h, Z and R.

$$\frac{\partial \hat{u}_g}{\partial Z_h} + \frac{\partial \hat{u}}{\partial Z_h} = 0 \tag{45}$$

$$Rf_1'(ZR) = \frac{\partial \hat{u}}{\partial Z}\ (Z,\ Z_h) = f_2(Z) \tag{46}$$

$$Zf_1'(ZR) = \frac{\partial \hat{u}_g}{\partial R}\ (R,Z_h) = f_3(R) \tag{47}$$

where the prime denotes total differentiation with respect to the argument. That f_2 is a function of Z only follows from the fact that the left side of (46) is independent of Z_h while the right side is independent of R; in a similar way, f_3 must be a function only of R. By similar reasoning, one can obtain from (46) and (47) together:

$$Zf_2(Z) = Rf_3(R) = \frac{1}{k} \tag{48}$$

where k is an undetermined constant that can be identified with the von Karman constant. With these substitutions, there result the solutions

$$\frac{u_g}{u_{*o}} = \frac{1}{k} [\ln R - A (Z_h)] \tag{49}$$

and

$$\frac{u}{u_{*o}} = \frac{1}{k} \ln z/z_o$$

By entirely analogous reasoning, one obtains

$$\frac{v_g}{u_{*o}} = - \frac{B(Z_h)}{k} \tag{50}$$

This reasoning shows that the Kazanski-Monin relations are quite generally valid provided the constants A and B are regarded as functions of hf/u_{*o}. These functions are not known at the present time. It is entirely possible that some of the scatter in the diagrams for A and B that Clarke has published is attributable to variations in h, which is generally not observed. The scatter is most serious in the determined values of B.

The occurrence of surface heating of the PBL introduces still one more variable, which can be selected to be the Monin-length

$$L_o = - \frac{c_p \rho T u_{*o}^3}{kg H_o} \tag{51}$$

where H_o is the surface heat flux. For purposes of nondimensionalizing it, it is immaterial whether we adopt ku_{*o}/fL_o, as is generally done, or h/L_o, as Deardorff (1972) has advocated, for either one can be derived from the other with the use of Z_h. To be consistent with general practice, we choose

$$\sigma = ku_{*o}/fL_o \tag{52}$$

which may be regarded as a kind of bulk planetary Richardson number.

The geostrophic defects now become functions of three independent variables

$$\frac{u - u_g}{u_{*o}} = \hat{u} \ (Z, \ Z_g, \ \sigma) \tag{53}$$

$$\frac{v - v_g}{u_{*o}} = \hat{v} \ (Z, \ Z_h, \ \sigma)$$

and

$$\frac{u_g}{u_{*o}} = \hat{u}\ (R,\ Z_h,\ \sigma)$$

$$\frac{v_g}{u_{*o}} = \hat{v}\ (R,\ Z_h,\ \sigma) \qquad (54)$$

From this point the reasoning proceeds in an entirely analogous way to the preceding discussion. The result is that the Kazanski-Monin constants must be regarded as functions of both kh/u_{*o} and σ to be determined from empirical data.

The behavior of A and B accompanying variations of σ have been studied by Clarke (1970). The observed values of A do not scatter appreciably, nor is there any significant variation from the mean value of about 5 for all values of σ in the range of -100 to -1000. Thus, under most typical unstable conditions, A may be regarded as being well known, even though the values of its arguments may be uncertain. It must be concluded that whatever the values of h may have been in Clarke's data, they had very little effect on the value of A. Since u_{*o} is determined primarily by A and is insensitive to B, it may be inferred that the presence of inversions that limit the height of the PBL do not normally have to be taken into account in the determination of u_{*o}.

Under stable conditions the scatter in A is much greater. Much of this scatter can be attributed to larger uncertainties in the determination of u_{*o} in these cases, as well as to the effects of accelerations and other disturbances. The possibility exists that the scatter might be reduced by taking h into account. More study of this problem is desirable.

---

*Calculations based on a two-layer model bounded above by an inversion show that the inversion height has only a negligible effect on A and B as long as it is situated above a height of $.15\ u_{*o}/f$.

The observed scatter in $B(\sigma)$ is enormous, and existing observations give little useful indication of the true form of this function. It is tempting to ascribe this scatter to the failure to stratify the data according to h. Since, however, B is mostly affected by the surface geostrophic drift angle α, is is most likely that the major portion of the scatter reflects the difficulty of measuring it and the sensitivity of this angle to local disturbances. Fortunately, u_{*_o} is insensitive to the value of $B(\sigma, Z_h)$ and so, the uncertainty of B is of no great concern for the prediction of u_{*_o}.

5.2 Practical Methods for Determining u_{*_o} and L_o from Large-Scale Variables

As we have seen, the surface drag coefficient $c_D = u_*/V_g$, the surface Rossby number and the stability parameter σ are connected by:

$$\ln(Ro) = A(\sigma) - \ln c_d + \left[\frac{k^2}{c_D^2} - B^2(\sigma)\right]^{1/2} \qquad (55)$$

Here $A(\sigma)$ and $B(\sigma)$ are universal functions recently measured by Clarke. Any effect of finite inversion height will be neglected. Here, σ is given by:

$$\sigma = \frac{ku_{*_o}}{fL_o} \qquad (56)$$

Empirically, $A(\sigma)$ and $B(\sigma)$ are well generated by

$$A(\sigma) = 4.5 \qquad \text{for } \sigma \leq -50$$

$$A(\sigma) = -14.4 \cdot 10^{-4}\,\sigma^2 - 14.4 \cdot 10^{-2}\,\sigma + 0.9 \qquad \text{for } \sigma > -50$$

$$B(\sigma) = 1.0 \qquad \text{for } \sigma \leq -75$$

$$B(\sigma) = 6.2 \cdot 10^{-4}\,\sigma^2 + 9.3 \cdot 10^{-2}\,\sigma + 4.5 \qquad \text{for } \sigma > -75$$

Since the geostrophic wind speed and the surface Rossby number can be assumed known, (55) will permit the estimation of the surface stress, provided σ is given. In practice, it is a nuisance to solve (55) numerically for c_D. Therefore, Figure 23 gives isopleths of σ as function of c_D and Ro which allows a graphical determination of c_D, given σ, V_g, and Ro. Also, once σ is known, L_o can be found from the definition of σ by (56). Before we can use Figure 23, we must first design methods for determining σ.

As a first approximation, we may assume that σ depends only on V_g and insolation, I.

Figure 24 shows how σ is related to these two variables. This figure is based on measurements at O'Neill (see Lettau and Davisdon, 1957), and Cape Kennedy. Of course, the graph can be used only during day time and between latitudes 25° and 45°. On windy nights, σ is almost zero and **turbulent** processes during lightwind nights play no important role and can be neglected.

Improvements may be possible, when measurements of the long-wave radiation of the earth's surface, for example from satellites, are available. Then, an estimate of the radiation balance during day and night-time hours can be found.

Where measurements of the incoming radiation are not available, it can be computed to a certain approximation (dependent on the variability of cloudiness) from known formulas from the date, the time of the day, the latitude and the cloudiness.

Some computations have shown that a quasi-empirical formula by Albrecht (see Möller, 1957) gives better agreement with measurements than the theoretical formula

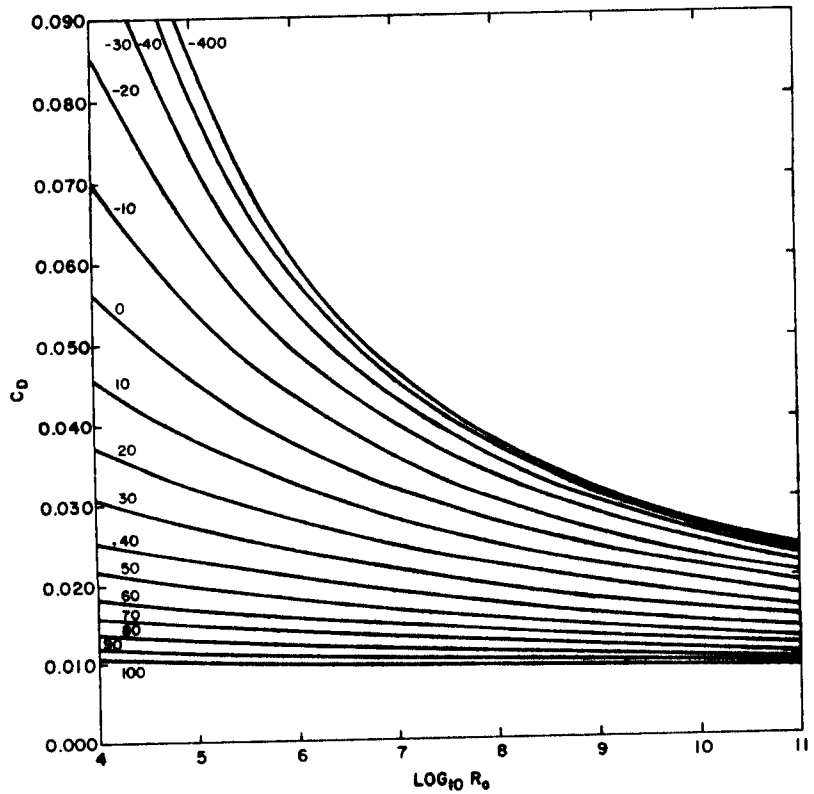

Figure 23. Geostrophic drag coefficient as function of σ and surface Rossby number.

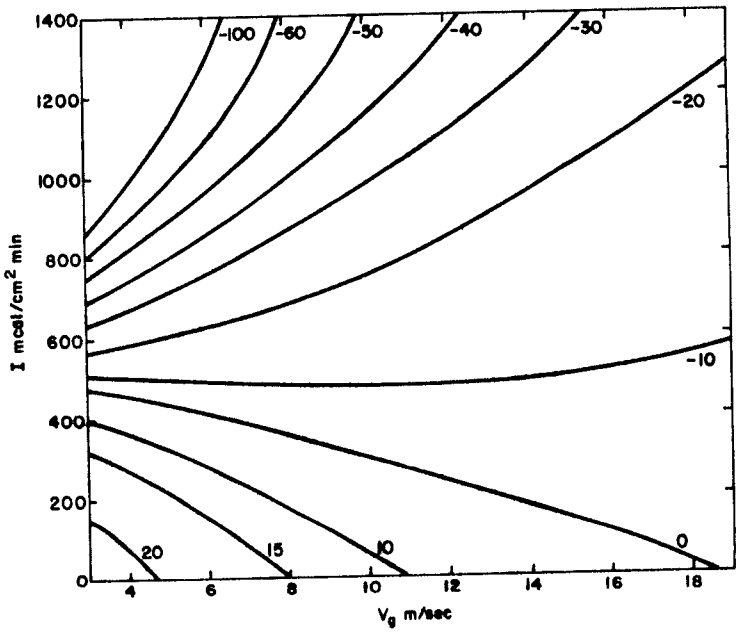

Figure 24. σ as function of insolation and geostrophic wind.

$$I = I_o \cos \zeta \, a^{\sec\zeta} \tag{57}$$

with I_o = solar constant

ζ = solar zenith angle

a = transmissivity.

Apparently, the difficulties lie in calculating the absorption of radiation. This absorption changes with the relative air mass and is dependent on wavelength. It is therefore a complicated function of the time in the day and location.

The mentioned formula by Albrecht reads

$$I = (I_o - I_w) \cos \zeta \, (1 - c \sqrt{M}) \, (1 + 1.19 \, A \, c \sqrt{\frac{p}{1000}}) \tag{58}$$

I_w = part which is absorbed by water vapor

M = absolute air mass (secant of zenith angle)

p = pressure in mb

A = albedo of the earth surface

c = backradiation constant (0.19 at Cape Kennedy)

For Cape Kennedy the simplification

$$I = 1585 \cos \zeta \, (1 - 0.19 \sqrt{M}) \tag{59}$$

gives values which for the present purpose are rather accurate. The very weak function of pressure $(1 + 1.19 \cdot c \sqrt{p/1000})$ has been contracted with $(I_o - I_w)$ into one constant.

For March 3, 1968, for example, the hourly mean values in Table 5 have been read off the radiation registrations from Cape Kennedy and have been compared with computed values from equation (59).

Table 5. Hourly Mean Values of Radiation at Cape Kennedy

Time LST	Measured Radiation m cal/cm^2 min	Calculated Radiation m cal/cm^2 min	ratio $\frac{I \text{ comp}}{I \text{ meas}}$
1200	1080	1100	1.02
1300	1090	1068	0.98
1400	1020	1012	0.99
1500	850	852	1.00
1600	620	626	1.01
1700	360	358	0.99
1800	95	98	1.03
1900	0	0	--

So far, this equation by Albrecht gives reliable values for the incoming radiation only when no clouds are present. If clouds are present, a correction factor has to be introduced.

Another possibility involving radiation measurements from satellites exists through use of the temperature θ_o of the earth's surface. Together with the temperature θ_g at the top of the boundary layer, the temperature difference $\Delta\theta = \theta_g - \theta_o$ can be used, instead of insolation, as an external parameter.

Equation (56) then can be written in the form

$$\sigma = \frac{g}{\theta} \frac{\Delta\theta}{fV_g} \frac{1}{c_D} \frac{T_*}{\Delta\theta} \tag{60}$$

Since both c_D and $T_*/\Delta\theta$ ($T_* = -\frac{1}{k} \frac{H}{\rho\, c_p\, u_*}$; scaling temperature) are functions of R_o and σ, σ can be expressed as

$$\sigma = f\ (S,\ R_o) \tag{61}$$

Here $S = \frac{g}{\theta} \frac{\Delta\theta}{fV_g}$ is a stability parameter given by external variables. By use of empirical data for the dependency of c_D and $T_*/\Delta\theta$ upon stability, the relationship given in equation (61) has been computed. The result is given in Figure 25. At high Rossby numbers and not too large values of S, σ is nearly independent upon R_o and varies only with S. Thus this second method also gives some justification for the assumption made for the construction of Figure 24. From the theoretical standpoint, the second method has some shortcomings. The known relationship for $\Delta\theta/T_*$ is most likely not correct

for Rossby numbers smaller than 10^5. The fact that this ratio changes sign for smaller Rossby numbers is the reason for intersecting σ lines at low S and R_o values. Intuitively, a theoretical relationship $\Delta\theta/T_*$ should approach asymptotically the lines S = 0 at small R_o numbers for all σ values. The derivation of such a relationship must remain the task for future work.

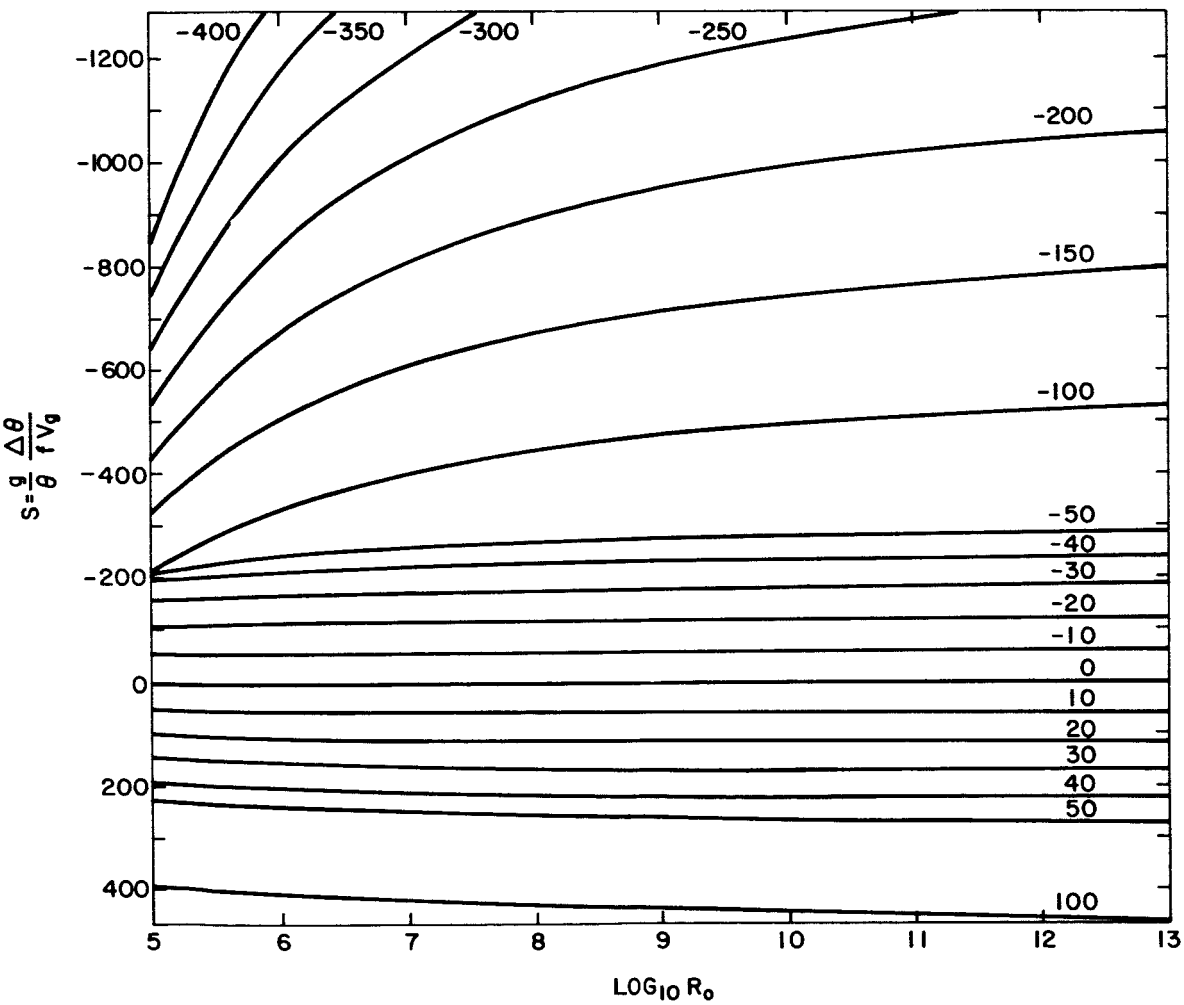

Figure 25. Stability parameter S as function of σ and surface Rossby number.

VI. DETERMINATION OF PREDICTANDS FROM LARGE-SCALE VARIABLES

6.1 Method

The purpose of this chapter is to test the computational scheme in which some of the statistics observed at the Kennedy tower are determined from "external" bulk variables. Equation (55) of Chapter V which gives the geostrophic drag coefficient $c_D = u_{*o}/V_g$ as a function of Rossby number Ro, and the planetary Richardson number σ, was solved by one of the methods suggested by Fielder (Chapter V).

First, Figure 24 is used to determine σ from I and V_g; then, c_D is determined from Figure 23. Given c_D, u_{*o} is known; L_o can then be found from u_{*o} and σ, given the definition of σ.

Values of geopotential height on the 850 mb surface prepared by the National Meteorological Center were obtained from the Nationl Center for Atmospheric Research archives in Boulder, Colorado. These 850 mb heights were available every 12 hours at 00 GMT and 12 GMT, on the regular NMC Northern Hemisphere grid which has a grid interval of 381 km at 60°N latitude.

Smoothed estimates of the geostrophic wind were obtained by

$$V_g = \frac{g}{f\Delta x} \sqrt{(\bar{z}_N - \bar{z}_S)^2 + (\bar{z}_W - \bar{z}_E)^2} \qquad (62)$$

in which Δx is the grid interval at Florida (301 km). $\bar{z}_N$ is the averaged value of the height at the two grid points north of Florida and $\bar{z}_S$, $\bar{z}_W$,

$\bar{z}_E$ and averaged values of height at the two grid points south, west and east of Florida. These geostrophic wind values were linearly interpolated to the tower site.

Insolation measurements, required for the determination of σ, were available at Cape Kennedy. However, inspection of these suggested that many of these were unrealistically low. Therefore, insolation was computed by the method discussed in the last chapter. The insolation was corrected for cloudiness by multiplying it by (1 - .03 C) where C is the cloudiness in tenths.

Figure 26 compares computed and observed insolations. Clearly, in many cases the observed values are unrealistic. This is further brought out by the fact that σ-values, estimated from these measurements, are often of the wrong sign. Therefore, in this test, σ was determined from Figure 24 as functions of computed insolation and measured geostrophic winds. Then, friction velocities were determined from Figure 23.

6.2 Test Results

The mean value of the friction velocities observed locally was 0.76 m/sec, about 77% larger than that calculated from V_g, 0.43 m/sec. The scattergram depicted in Figure 27 illustrates the relationship between the two sets of u_{*_o}. Some positive correlation is evident. The large amount of scatter is probably due to the uncertainty in the geostrophic wind calculations. The systematic difference could easily be due to the fact that an average geostrophic wind in a $(300\ km)^2$ area is systematically smaller than the

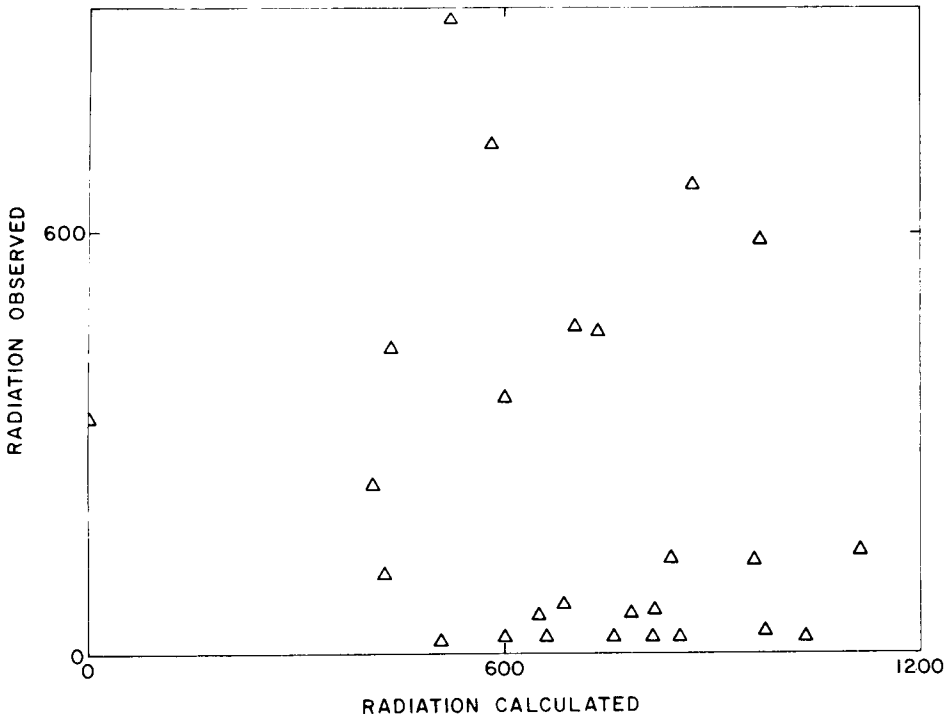

Figure 26. Comparison of observed and computed insolation, in 1000 ly min^{-1}.

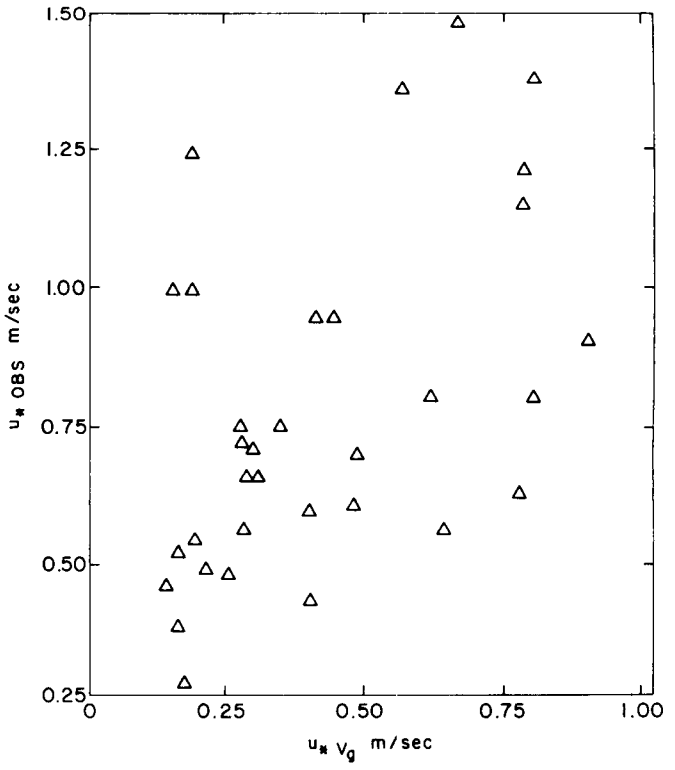

Figure 27. Comparison of u_{*_o} derived from geostrophic wind vs u_{*_o} from local data.

local geostrophic wind over Cape Kennedy, particularly, if the average is small. Note that the discrepancy disappears for large speeds, where one might expect smaller systematic differences between the two kinds of wind.

Another difficulty arises from the uncertainty in the roughness lengths already discussed in earlier chapters. Both sets of u_{*_o} compared in Figure 26 are based on the same z_o's, namely those derived in Chapter II. As we have seen, these roughness lengths are too large to account for the statistical fluctuations of the winds at Cape Kennedy.

Now it turns out that the u_{*_o}'s estimated from V_{18} are much more sensitive to the assumed z_o's than those based on geostrophic winds. Therefore the question was raised what values of z_o would eliminate the systematic differences between the two sets of u_*. These turned out to be two orders of magnitude less than the observed z_o's, and therefore are quite unrealistic. It is concluded that it is impossible to ascribe the systematic differences between abscissa and ordinate in Figure 27 to incorrect roughness lengths; as suggested above, the explanation can be found more probably in the significantly underestimation of <u>local</u> geostrophic winds.

We shall assume that the u_{*_o}'s obtained from the winds at 18 m are correct. Hence, the best estimate of u_{*_o}, given geostrophic winds, would be based on the line of regression fitting Figure 27.

$$u_{*_o\ est} = 0.51 + 0.62\ u_{*_o}\ (V_g, \sigma) \qquad (63)$$

These estimates should then form the basis for obtaining wind profiles eq. (15) and ε (eq. (28)) and standard deviations. Test of this

suggestion should be made at other locations since there is no guarantee that eq. (63) is generally valid.

Figure 28 is a plot of u_{*o} (V_g, σ) calculated from V_g as abscissa and the standard deviation of the longitudional fluctuation σ_u, as ordinate. The average value of σ_u/u_{*o} (V_g, σ) which agrees quite well with observations made at other tower sites (see Lumley and Panofsky, 1964). Again, most of the scatter is probably due to the uncertainty in the geostrophic wind observations. The large scatter in Figure 28 suggests that the best agreement with observed standard deviations at Kennedy is obtained by fitting a line of regression to Figure 27:

$$\sigma_u = 0.80 + 0.77\ u_{*o}\ (V_g, \sigma) \tag{64}$$

Similarly, for the lateral component, at 18 m

$$\sigma_v = 0.92 + 0.37\ u_{*o}\ (V_g, \sigma) \tag{65}$$

But, as we have suggested, there are strong indications that the observed quantities are too small. It is proposed that a better procedure for estimating σ_u and σ_v from geostrophic winds, roughness lengths and stability information is to use an equation like (63) to estimate u_{*o} and then multiply by 2.5 and 2.2, respectively, to obtain σ_u and σ_v. This technique will be tested on observations to be made at Risø, Denmark, on the 125 m tower.

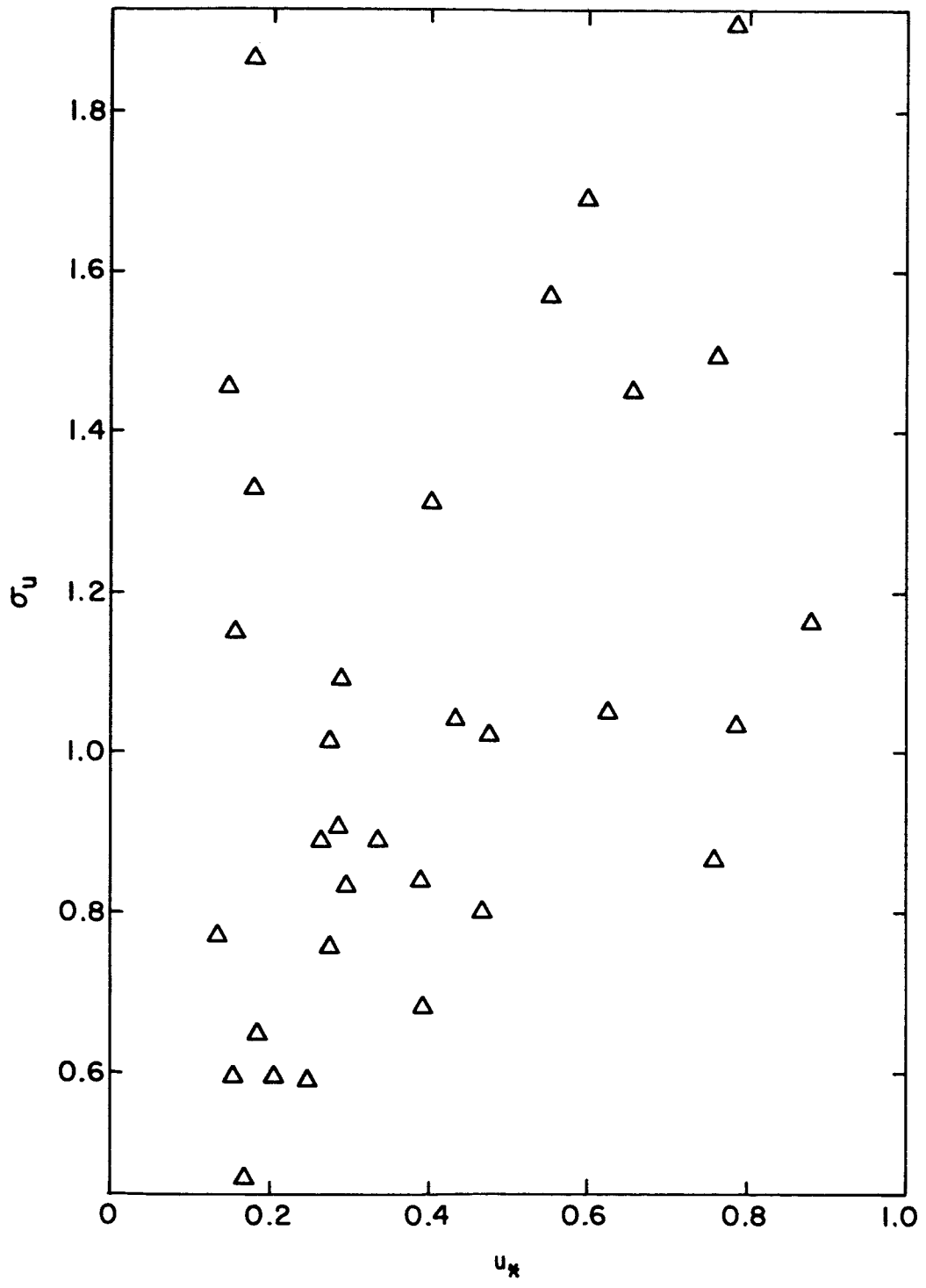

Figure 28. σ_u as function of u_{*_o} derived from geostrophic wind.

Still, all estimates based on geostrophic winds are certain to have large random errors even if the systematic errors can be eliminated, for the correlation coefficient between observed standard deviations and u_{*_o} computed from geostrophic wind is only about 0.44 for the u-component and 0.24 for the v-component. As we have seen in Chapter IV, correlation coefficients are about twice as large between standard deviations and u_{*_o}'s obtained from local wind. Hence, standard deviations should be estimated from local rather than geostrophic wind if at all possible.

VII. SUMMARY OF PRACTICAL METHODS FOR ESTIMATION OF LOW-LEVEL WIND STATISTICS

7.1 Roughness Length, Friction Velocity and L_o When Large-Scale Information Only Is Available

a. Daytime. When there is only large-scale information, local statistics can be estimated from the three basic quantitites: geostrophic wind speed, insolation and roughness length.

The roughness lengths need not be extremely accurate and can be estimated from the local terrain according to the following table:

Table 6. Roughness lengths for various terrain types, in cm.

Ocean or ice	0.01
Smooth grass	1
Rough grass	5
Farm land, smooth	10
Farm land, rough	50
Forest, cities	200

Insolation with clear sky can be determined from the usual astronomical formulae, or, if Cape Kennedy is typical, from:

$$I = 1.585 \cos \zeta \ (1 - 0.19 \sqrt{\sec \zeta})$$

Here, I is the insolation in ly/min and ζ is the zenith distance of the sun, which can be computed from hour angle t, declination of the sun δ and latitude ϕ by

$$\cos \zeta = \cos t \cos \delta \cos \phi + \sin \delta \sin \phi$$

In cloudy skies, this estimate has to be multiplied by (1 - .01 aC) where C is the cloudiness in tenths and a depends on the type of cloud. We have used a = 3, though the value should be considerably larger (perhaps 7) with low clouds.

Given I and the geostrophic wind, V_g, the planetary Richardson number σ is obtained from Figure 24. Hence, the surface stress is found from Figure 23, given σ and the geostophic wind. If the Kennedy results are representative, a better estimate of friction velocity is finally found from

$$u_{*o} = 0.51 + 0.62\ u_{*o}(V_g, \sigma)$$

where $u_{*o}(V_g, \sigma)$ is the friction velocity obtained from σ and V_g.

Next the Pasquill class is determined from Table 2. For this table, we need a rough estimate of wind speed. This is given sufficiently accurately by the logarithmic wind law applied at 10 m:

$$u = \frac{u_{*o}}{k} \ln \frac{10\ m}{z_o}$$

Radiation is taken to be weak if less than 0.5 ly/min, medium if between 0.5 and 1.0 ly/min, and strong if greater than 1.0 ly/min.

Finally, Figure 9 gives an estimate of L_o, from Pasquill class and roughness length. We now have u_{*o}, z_o, and L_o and can proceed to Section 7.3 of this chapter.

b. Night. At night, large-scale variables are not likely to yield good estimate of L_o and friction velocity, unless winds are too strong and stratification near neutral. The following procedure is recommended, but has not been tested. First, obtain roughness length as in (a). Then, determine a first approximation of surface friction velocity from Figure 23, assuming $\sigma = 0$. This approximation will be good in strong winds, but too large in weak-wind cases with strong inversions. In any case, use the logarithmic law applied at 10 m to obtain a rough wind speed. Use this to determine Pasquill class from Table 2. Figure 9 gives the first estimate of L_o, as function of roughness length and Pasquill class.

Given L_o and u_{*o}, we can now estimate the planetary Rossby number from its definition:

$$\sigma = \frac{0.4\ u_{*o}}{f\ L_o}$$

With this and geostrophic wind, we enter Figure 23 and obtain a second estimate of surface friction velocity. This procedure can then be iterated until it converges. It is expected that it will be fairly reliable under near-neutral conditions, but not in very stable air. But in the latter case, the winds are likely to be too weak to be of practical consequence.

Again, a better estimate of u_{*o} can be found from

$$u_{*o} = 0.51 + 0.62\ u_{*o}(V_g, \sigma)$$

if the Kennedy results are typical. We then proceed to Section 7.3.

7.2 Friction Velocity and L_o from Low-Level Data

It is expected that better estimates of surface friction velocity and L_o can be obtained when a low-level wind is measured (e.g., given from hourly sequences) than if geostrophic winds have to be used. First, roughness length is estimated as before. Next, the Pasquill class is found from Table 2. Pasquill class and roughness length yield L_o according to Figure 9.

The surface friction velocity can now be found from the equation for the wind profile:

$$u_{*o} = \frac{0.4\ u}{\ln z/z_o - \psi\ (z/L_o)}$$

where ψ is tabulated in Table 1. It is recommended that the height z be taken as 10 m, the height recommended for synoptic wind observations. This method has not been tested.

7.3 Estimation of Various Statistics from z_o, L_o and u_{*o}

a. Wind Profile. The wind profile up to 150 m or so is well described by

$$u = 2.5\ u_{*o}\ [\ln\ (\frac{z}{z_o}) - \psi\ (\frac{z}{L_o})]$$

where ψ is given in Table 1.

b. Variance. At this point, it is recommended that, at all levels, up to 150 m

$$\sigma_u = 2.5\ u_{*o}$$

and

$$\sigma_v = 2.2\ u_{*o}$$

These equations are not so much based on Kennedy results, but on average results at various locations. Correction for height or stability appears premature, since no generally valid behavior has been documented.

c. Spectra at high frequencies. At high frequencies ($n > u/z$), the inertial-subrange formulae appear valid:

$$S(n) = c\ \varepsilon^{2/3}\ u^{2/3}\ n^{-5/3}$$

Here, ε is the dissipation of turbulence into heat and the constant, c, is .14 for the u-component and .18 for the v-component, n is the frequency.

At 30 m and above, ε is estimated by:

$$\varepsilon = \frac{2.5\ u_{*o}^{3}}{z}\ [(1 - 16\ z/L_o)^{1/4} - \frac{z}{L_o}]$$

and, below, 30 m, by

$$\varepsilon = \frac{2.5\ u_{*o}^{3}}{z}\ [1 - 16\ z/L_o)^{-1/4}$$

d. Coherence. Coherence in the vertical is given by:

$$\text{coh}(n) = e^{-K\ n\Delta z/u}$$

where Δz is the height difference between the two levels considered. K is a decay constant which depends on z/L_o as shown in Figures 19 and 20.

The "slope" S, defined by

$$S = \frac{V}{2\pi\ n\Delta z}\ \text{arc tan}\ (Q/C)$$

(Q, quadrature spectrum; C, cospectrum) is about 1 for longitudional and 2 for lateral velocity components below 100 m and half as large between 100 m and 150 m.

Tests of all these procedures at locations away from Cape Kennedy are urgently needed to test the generality of these methods.

REFERENCES

Blackadar, A. K., 1962: The vertical distribution of wind and turbulent exchange in a neutral atmosphere. J. Geophys. Res., 67, 3095-3102.

Blackadar, A. K., 1965a: A single-layer theory of the vertical distribution of wind in a baroclinic neutral atmopsheric boundary layer. Pp. 1-22 in Final Report Contract AF(604)-6641. The Pennsylvania State University, (AFCRL-65-531), 140 pp.

Blackadar, A. K., 1965b: A simplified two-layer model of the baroclinic neutral atmospheric boundary layer. Pp. 49-65 in Flux of Heat and Momentum in the Planetary Boundary Layer of the Atmosphere. Final Report, Contract AF(604)-6641, The Pennsylvania State University, 140 pp.

Blackadar, A. K., and H. A. Panofsky, 1969: Flow similarity in diabatic boundary layers. Pp. 47-56 in Wind Profiles, Spectra, and Cross-Spectra over Homogeneous Terrain. Final Report, Contract DA-28-043-AMC-01388(E), The Pennsylvania State University, 71 pp.

Blackadar, A. K. and H. Tennekes, 1967: External parameters of the wind flow in the barotropic planetary boundary layer of the atmopshere. App. IV (9 pp.) of Global Atmospheric Research Programme, Report of the Stockholm Study Conference; ICSU-IUGG Comm. on Atm. Sci. and the World Meteor. Org.

Blackadar, A. K. and H. Tennekes, 1968: Asymptotic similarity in neutral barotropic planetary boundary layers. J. Atmos. Sci., 25, 1015-1020.

Businger, J. A., J. C. Wyngaard, Y. Izumi and E. F. Bradley, 1971: Flux profile relationships in the atmospheric surface layer. J. Atmos. Sci., 28, 181-189.

Clarke, R. H., 1970: Observational studies in the atmospheric boundary layer. Quart. J. Roy. Meteor. Soc., 96, 91-114.

Csanady, G. T., 1967: On the resistance law of a turbulent Ekman layer. J. Atmos. Sci., 24, 467-471.

Davenport, A. G., 1961: The spectrum of horizontal gustiness near the ground in high winds. Quart. J. Roy. Met. Soc., 194-211.

Deardorff, J. W., 1972: Numerical investigation of neutral and unstable planetary boundary layers. J. Atm. Sci., 29, 91-115.

Elliott, W. P., 1958: The growth of the atmospheric internal boundary layer. Trans. Amer. Geophys. Un., 39, 1048-1054.

Fichtl, G. H. and G. E. McVehil, 1970: Longitudinal and lateral spectra of turbulence in the atmospheric boundary layer at the Kennedy Space Center. J. Appl. Meteor., 9, 51-63.

Gill, M. E., 1967: The turbulent Ekman layer. Dept. Appl. Math. and Theor. Phys., University of Cambridge, England (unpublished manuscript).

Golder, D., 1972: Relations among stability parameters in the surface layer. Bound. Layer Meteor. 3, 47-58.

Kazanski, A. B. and A. S. Monin, 1961: On the dynamical interaction between the atmopshere and the earth's surface. Bulletin Acad. Sci., U.S.S.R., Ser. Geophys., No. 5, 786-788.

Lettau, H. and B. Davidson, ed., 1957: Exploring the Atmosphere's First Mile. Vol. I, Instrumentation and Data Evaluation; Vol. II, Site Description and Data Tabulation; Pergamon, 578 + xiv pp.

Lumley, J. L. and H. A. Panofsky, 1964: The Structure of Atmospheric Turbulence. John Wiley, N. Y., 239 + xi pp.

Möller, F., 1957: Strahlung in der unteren Atmosphäre. Handbuch der Physik Vol. 48, 155-253, Springer Verlag, Berlin.

Monin, A. S. and S. S. Zilitinkevich, 1967: Planetary boundary layer and large-scale atmospheric dynamics. Appendix V (37 pp.) of Global Atmospheric Research Programme, Report of the Stockholm Study Conference; ICSU-IUGG Committee on Atmospheric Sciences-WMO.

Panofsky, H. A., 1962: The budget of turbulent energy in the lowest 100 meters. J. Geophys. Res., 67, 3161-3165.

Panofsky, H. A., 1963: Determination of stress from wind and temperature measurements. Quart. J. Roy. Met. Soc., 89, 85-94.

Panofsky, H. A., and E. L. Petersen, 1972: Wind profiles and change of terrain roughness at Risø. Quart. J. Roy. Met. Soc., 98, 845-854.

Paulson, C. A., 1970: The mathematical representation of wind speed and temperature profiles in the unstable atmospheric surface layer. J. Appl. Met., 9, 857-861.

Slade, D. H., ed., 1968: Meteorology and Atomic Energy. U. S. Atomic Energy Commission, 445 + x pp.

Thuillier, R. H. and V. O. Lappe, 1964: Wind and temperature profile characteristics from observations on a 1400 ft. tower. J. Appl. Met., 3, 299-306.

Wyngaard, J. C. and O. R. Coté, 1971: The budgets of turbulent energy and temperature variance in the atmopsheric surface layer. J. Atmos. Sci., 28, 190-201.